Nature of slab-mantle interactions recorded by coupled $\delta^{13}C$–$\delta^{15}N$–$\delta^{18}O$ signatures and elemental compositions of Koidu diamonds and their inclusions

Mei Yan Lai [a,*] (meiyan1@ualberta.ca),

Thomas Stachel [a] (tstachel@ualberta.ca),

Richard A. Stern [a] (rstern@ualberta.ca),

Kan Li [a] (kan3@ualberta.ca),

D. Graham Pearson [a] (gdpearso@ualberta.ca),

Jeff W. Harris [b] (jeff.harris@glasgow.ac.uk)

[a] Department of Earth and Atmospheric Sciences, University of Alberta, Edmonton, Canada

[b] School of Geographical and Earth Sciences, University of Glasgow, Glasgow, United Kingdom

* Corresponding author

Abstract

Eclogitic diamond formation can be associated with interactions between subducted slabs and ambient mantle. To gain a better understanding of the extent of chemical exchange between slabs and ambient mantle and the mechanisms of coeval diamond formation, we examined 16 diamonds with eclogitic garnet inclusions from the Koidu kimberlite complex in Sierra Leone (West African Craton). We analyzed the 16 garnet inclusions for major element, trace element and oxygen isotope ($\delta^{18}O$) compositions and their host diamonds for carbon ($\delta^{13}C$) and nitrogen ($\delta^{15}N$) isotope compositions.

The garnet inclusions have $\delta^{18}O$ values ranging from +5.4 to +12.1 ‰ (median = +11.3 ‰) and all but two have $\delta^{18}O$ values ≥ +9.9 ‰. Such high $\delta^{18}O$ values indicate a link to protoliths that had undergone extensive low-temperature alteration by seawater, which occurs in the uppermost basaltic layer of oceanic crust, prior to subduction. Diamonds hosting the high $\delta^{18}O$ garnets have a crustal $\delta^{13}C$ signature (-29.6 to -19.4 ‰) paired with $\delta^{15}N$ values (-5.6 to +1.3 ‰, with one outlier at +9.9 ‰) implying typically only minor ^{15}N enrichment. This apparent decoupling of $\delta^{18}O$ and $\delta^{13}C$ from $\delta^{15}N$ indicates diamond formation in an eclogitic substrate where garnet oxygen isotope compositions are inherited from altered low-pressure protoliths, diamond carbon is principally derived from biogenic carbonate and organic matter, and diamond nitrogen is variably added by an external, mantle-derived fluid that prompted diamond formation. Of the two remaining garnet inclusions, one has mantle-like $\delta^{18}O$ (+5.4 ‰) and a positive Eu anomaly, suggesting derivation from gabbroic protoliths originally located deep in the oceanic crust where significant alteration by seawater did not occur. Based on mantle-like $\delta^{13}C$ (-4.7 ‰) and $\delta^{15}N$ (-6.9 ‰), the associated diamond formed from mantle-derived fluids/melts. Relative to the other Koidu garnet inclusions, the final garnet has a small majorite component (formation pressure ~ 8 GPa), high Mg# (79.0), elevated Cr# (0.90), and low $\delta^{18}O$ (+6.3 ‰), suggesting encapsulation during infiltration of slab-derived melts into surrounding asthenospheric

peridotite, associated with a high degree of chemical exchange between slab- and mantle-derived components.

Keywords: Eclogitic diamond; carbon isotope; nitrogen isotope; oxygen isotope; slab-mantle interaction

1. Introduction

Despite the minor proportion of eclogite within the lithospheric upper mantle (< 1 vol%; Schulze, 1989), eclogite xenoliths provide key information about past geodynamic processes. Subduction and associated metamorphism of oceanic crust in the mantle (Helmstaedt and Doig, 1975; MacGregor and Manton, 1986; Jacob, 2004) has been widely accepted as the origin of most, if not all, mantle eclogite xenoliths. Alternate models that invoke direct crystallization from basaltic melts produced from peridotites in the deep mantle (O'Hara and Yoder, 1967; McGetchin and Silver, 1972; Caporuscio and Smyth, 1990) are inconsistent with the major and trace element relationships observed in eclogite xenoliths (Aulbach and Arndt, 2019). In addition, Eu anomalies and oxygen isotope signatures in eclogites are unambiguous evidence for a crustal origin.

Europium anomalies in the rare earth element (REE) patterns of eclogite whole rocks or their mineral constituents indicate that the formation of their protoliths involved accumulation or fractionation of plagioclase – a low-pressure mineral formed in Earth's crust. Since plagioclase preferentially incorporates Eu from melts relative to other REEs (Weill and Drake, 1973; Bédard, 1994), cumulate gabbros, cumulate-enriched in plagioclase that crystallized in the lower oceanic crust, often have positive Eu anomalies. This results in depletion of Eu in the residual melts, which subsequently may rise into the upper oceanic crust to form basalts with negative Eu anomalies (Philpotts and Schnetzler, 1968).

Since some eclogites do not have discernible Eu anomalies (Jacob, 2004; Schmickler et al., 2004), fractionated oxygen isotope compositions are often used to infer a crustal protolith. Peridotitic mantle has a very restricted oxygen isotope composition ($\delta^{18}O$) of +5.5 ± 0.4 ‰ (Mattey et al., 1994; Regier et al., 2018), whereas oceanic crust has a much wider range from 0 to +15 ‰ (Eiler, 2001; Korolev et al., 2018). Oceanic crust with $\delta^{18}O$ values above or below the peridotitic mantle range is attributed to low-temperature (< 150 °C) submarine weathering or high-temperature (> 350 °C) hydrothermal alteration, respectively. Low-temperature weathering occurs at or near the seawater–basalt interface, while high-temperature alteration occurs in the deeper portion of oceanic crust (Muehlenbachs and Clayton, 1972a,b; Gregory and Taylor, 1981; McCulloch et al., 1981; Alt et al., 1986). Previous studies have shown that the $\delta^{18}O$ values inherited from these processes are generally retained by eclogites metamorphosed from subducted oceanic crust (Putlitz et al., 2000; Jacob, 2004; Russell et al., 2013). The high $\delta^{18}O$ values in eclogites cannot be formed by isotopic fractionation at mantle temperatures from an initial mantle-like value (+5.5 ± 0.4 ‰) (Mattey et al., 1994; Schulze et al., 2013; Regier et al., 2018) nor by mantle metasomatism, as metasomatic fluids with extreme $\delta^{18}O$ values are not likely to survive unmodified during passage through the dominantly peridotitic mantle (Riches et al., 2016).

Garnet is the preferred proxy for the determination of the oxygen isotope composition of eclogites as it is more resistant than clinopyroxene to metasomatic modification and resetting of its isotopic composition (Jacob et al., 1994; Deines and Haggerty, 2000; Schulze et al., 2000; Barth et al., 2001; Korolev et al., 2018). In this study, we analyse garnet inclusions in diamonds from the Koidu kimberlite complex in Sierra Leone for their major element, trace element and stable isotope compositions. Eclogitic diamond formation could be associated with interactions between eclogite and ambient mantle: (1) eclogite-derived carbonated melts may migrate into reducing ambient mantle

peridotite and precipitate diamonds (Rohrbach and Schmidt, 2011; Kiseeva et al., 2013; Mikhail et al., 2021); (2) partial melting of eclogite may facilitate *in situ* diamond formation as well as chemical exchange with surrounding peridotite (Smart et al., 2009); (3) mantle-derived fluids/melts may interact with eclogitic diamond substrates (Aulbach et al., 2011; Lai et al., 2022). Thus, correlations between $\delta^{18}O$ values and major element compositions of garnet inclusions may provide insights into the degree of slab-mantle interaction during diamond formation. Carbon ($\delta^{13}C$) and nitrogen ($\delta^{15}N$) isotope compositions of the host diamonds of these garnet inclusions are analysed to identify any mixing of crust- and mantle-derived carbon and nitrogen during this process. Here we present the first coupled $\delta^{13}C$–$\delta^{15}N$–$\delta^{18}O$ measurements of diamonds and their inclusions, to gain a better understanding of the nature of the interaction between subducted slabs and ambient mantle during diamond formation.

2. Samples and methods

The Koidu kimberlite complex is situated in the Kono District of eastern Sierra Leone, in the southern part of the West African Craton. Although eclogites are the only type of mantle xenoliths recovered from Koidu (Tompkins and Haggerty, 1984; Hills and Haggerty, 1989; Fung and Haggerty, 1995), kimberlite indicator minerals and diamonds from this locality are of both peridotitic and eclogitic paragenesis (Deines and Harris, 1995; Skinner et al., 2004; Harder et al., 2013).

A mineral chemistry study on 105 Koidu diamonds revealed a dominance of eclogitic diamonds (78%), followed by lesser proportions of peridotitic (17%) and mixed paragenesis diamonds (containing co-occurring peridotitic and eclogitic mineral inclusions; 5%) (Lai et al., 2022). Sixteen eclogitic garnet inclusions from 15 different eclogitic diamonds and one mixed paragenesis diamond were selected for the determination of their oxygen isotope composition. The selected garnets cover the entire major

element compositional range for all Koidu eclogitic garnet inclusions, and thus are representative of the sample suite.

Methods for determining major, minor and trace element compositions of mineral inclusions were previously described in detail (Lai et al., 2022) and are only summarised here. Garnet inclusions were mounted in epoxy and analysed with a CAMECA SX100 electron probe microanalyzer (EPMA) for their major and minor element compositions at an accelerating voltage of 20 kV, a beam current of 20 nA, and a fully focused beam with a diameter < 1 µm. Oxide detection limits are typically ≤ 0.02 wt%. Subsequently, trace element compositions of garnet inclusions were determined using a Resonetics M-50-LR 193 nm ArF excimer laser ablation system coupled with a Thermo Scientific Element IIXR inductively coupled plasma mass spectrometer (LA-ICP-MS). Samples were ablated with a spot size of 23–90 µm at a frequency of 10 Hz and a laser fluence of ~4 J/cm^2. Calcium contents of garnet inclusions determined with EPMA were used as internal standard. Detection limits for trace element concentrations are typically ≤ 40 ppb for REE, V, Rb, Sr, Zr, Nb, Ba and Hf, and ≤ 1 ppm for Ti and Ni.

Selected eclogitic garnet inclusions were subsequently co-mounted into a single 25 mm epoxy mount with reference materials S0068 (pyrope garnet from the Gore Mountain area; Bartholomé, 1960) and S0088B (grossular garnet from the Jeffrey mine; Akizuki, 1989). The epoxy mount was polished and coated with 25 nm of Au prior to scanning electron microscopy (SEM). Secondary electron (SE) and backscattered electron (BSE) images were obtained using a Zeiss EVO MA15 SEM operating at a voltage of 20 kV and a beam current of 3–4 nA. After imaging, the epoxy mount was coated with 100 nm of Au. Oxygen isotope compositions were then determined using a CAMECA IMS-1280 multi-collector ion microprobe. Three to six spots were analysed on each garnet inclusion to assess compositional homogeneity. A $^{133}Cs^+$ primary beam with an impact energy of 20 keV and a beam current of 2 nA was focused to a beam diameter of approximately 12 µm. Analysis of each spot took

240 s. Oxygen isotope compositions are reported as $\delta^{18}O_{VSMOW}$ [normalized difference of the $^{18}O/^{16}O$ ratio of the sample relative to that of Vienna Standard Mean Ocean Water (VSMOW), where $^{18}O/^{16}O_{VSMOW}$ = 2005.20 (±0.45) × 10^{-6} (Baertschi, 1976)]. Reference materials S0068 (with $\delta^{18}O_{VSMOW}$ = +5.72 ‰) and S0088B (with $\delta^{18}O_{VSMOW}$ = +4.13 ‰) were analysed after every four and eight unknowns, respectively, to monitor the instrumental mass fractionation (IMF). The 95% confidence uncertainty estimates for $\delta^{18}O_{VSMOW}$ of analysed garnet inclusions average ±0.26 ‰, which include errors related to within-spot counting statistics, between-spot (geometric) effects, correction for IMF, and matrix effects associated with Ca# (i.e., molar Ca/(Ca+Mg+Fe)). Details of the analytical procedure and matrix calibration are outlined in supplementary information and references therein.

3. Results

3.1 Major element composition

The selected garnet inclusions show large variations in CaO (3.6–18.6 wt%), MgO (8.5–20.6 wt%), FeO (9.0–18.6 wt%) and Mg# (49.1–79.0), with the garnet (138-7-3) from a mixed paragenesis diamond having the highest CaO and lowest MgO and FeO (Table 1). The garnet (140-2-1) with the highest MgO content also has the highest TiO_2 concentration (0.86 vs 0.24–0.48 wt% in other garnets). The high Ti in this garnet does not correspond to its relatively low Na_2O (0.13 wt%). Typically, Na increases with Ti in garnet (Fig. 1), corresponding to the coupled substitution: $M^{2+} + Al^{3+} = Na^{+} + Ti^{4+}$ (Ringwood and Major, 1971; Bishop et al., 1976, 1978; Grew et al., 2013), however, this positive correlation is not observed for majoritic garnets (Stachel et al., 1998). The concentration of Ti in garnet increases with temperature (Aulbach, 2020) and consequently with pressure, along a conductive geotherm. This agrees with high pressure-high temperature experiments showing that Ti in garnet

increases with both temperature and pressure (Zhang et al., 2003). This garnet also has relatively low Al_2O_3 (21.1 wt%) compared with the average Al_2O_3 content (22.9 wt%) of other garnets in this study. A negative correlation ($R^2 = 0.81$; n = 16) between Al and Ti cations is observed for garnet inclusions from Koidu diamonds (Fig. 2), which is consistent with experimental results documenting decreasing Al and increasing Ti with increasing temperature and pressure (Zhang et al., 2003), following the coupled substitution: $2Al^{3+} = M^{2+} + Ti^{4+}$ (Ackerson et al., 2017). In agreement, garnet 140-2-1 has a minor majorite component of 3.4 mol% (calculated following Locock, 2008). Compared to Si and Al + Cr cation contents in experimental majoritic garnets (Akaogi and Akimoto, 1979; Irifune et al., 1986; Irifune, 1987; Collerson et al., 2010), a pressure of 7.8 GPa (corresponding to a depth of 250 km) (Fig. 3) is estimated for this garnet. Applying different formulations of the majorite-in-garnet barometer (Collerson et al., 2010; Beyer and Frost, 2017) yields equilibration pressures of 7.8–8.2 GPa, corresponding to a depth between 250 and 260 km. This depth range is slightly below the lithosphere-asthenosphere boundary of the West African Craton (220 ± 10 km), determined from Koidu clinopyroxene xenocryst geothermobarometry (Smit et al., 2016). Backscattered electron imaging of garnet 140-2-1 shows no exsolution, suggesting that it did not re-equilibrate at shallower depth, and was brought to the surface directly from the uppermost asthenosphere.

3.2 Trace element composition

Koidu eclogitic garnet inclusions are depleted in LREE with subchondritic La, which is a typical feature observed in eclogitic garnets from mantle xenoliths (Jacob, 2004) and included in diamonds (Stachel et al., 2004) worldwide. The garnet (138-7-3) from the mixed paragenesis diamond is distinct in having the highest LREE (La_N ~0.3) and lowest HREE (Lu_N ~6) contents. The remaining garnets have flat $MREE_N$-$HREE_N$ with $Lu_N > 20$ (Table 2), and among them, the mildly majoritic garnet 140-2-1 has the highest LREE and lowest HREE.

Three garnets (131-5-8, 138-6-2 and 138-12-1) have negative Eu anomalies (Fig. 4a), with $[Eu/Eu^*]_N$ = 0.80–0.89, where $Eu^* = [Sm_N \times Gd_N]^{0.5}$ (McLennan, 1989). Garnet 138-7-3 has a small positive Eu anomaly ($[Eu/Eu^*]_N$ = 1.10), but two additional garnet inclusions from the same diamond have more prominent positive Eu anomalies ($[Eu/Eu^*]_N$ = 1.36–1.41). All other garnets in this study lack discernible Eu anomalies (Fig. 4b).

3.3 Oxygen isotope composition

Backscattered electron images and multiple spot analyses indicate that all garnet inclusions in this study have homogeneous compositions, which excludes the possibility of alteration by fluid/melt infiltrating through cracks in their host diamonds. The internal variability of $\delta^{18}O$ for individual grains (average 2σ = 0.17 ‰) is within analytical uncertainty (2σ = ~0.26 ‰), thus only average $\delta^{18}O$ values are reported for each grain (Table 3) and used for discussion in the following section. Oxygen isotope compositions for all analyzed spots are provided in Table S1.

The range of $\delta^{18}O$ values of garnet inclusions in this study (+5.4 to +12.1 ‰; Fig. 5) is much greater than that of garnets from the Koidu low-MgO (+4.7 to +6.8 ‰) and high-MgO (+5.1 to +5.7 ‰) eclogite xenoliths (Barth et al., 2001, 2002). Garnet 138-7-3 from the mixed paragenesis diamond has the lowest $\delta^{18}O$ value (+5.4 ‰), falling within the mantle range (+5.5 ± 0.4 ‰; Mattey et al., 1994). The mildly majoritic garnet 140-2-1 also has a relatively low $\delta^{18}O$ value (+6.3 ‰). The other garnets in this study have $\delta^{18}O$ values from +9.9 to +12.1 ‰, with a median value of +11.6 ‰, which is higher than that of any other eclogitic garnet inclusion in lithospheric diamonds worldwide, including diamonds from the Damtshaa kimberlites (+4.7 to +8.8 ‰; Ickert et al., 2013), Argyle lamproite (+6.0 to +8.3 ‰; Schulze et al., 2013), Finsch kimberlite (+5.7 to +8.0 ‰; Lowry et al., 1999), Siberian placer deposits (+4.8 to +9.6 ‰; Zedgenizov et al., 2016), Jericho kimberlite (+5.2 to +6.0 ‰; Smart et al., 2012) and Guaniamo placer deposit (+7.9 to +11.3 ‰; Schulze et al., 2004) (Fig. 6).

A negative correlation between $\delta^{18}O$ values and Mg# (molar 100×Mg/(Mg+Fe)) and a positive correlation between $\delta^{18}O$ values and Ca# (molar 100×Ca/(Ca+Mg+Fe)) are observed in some garnets (Fig. 7a and b). These correlations are especially obvious for three garnets (138-3-1, 138-5-1 and 138-11-1) that also show decreasing LREE contents with decreasing Ca# (Fig. 4b). Garnets with the highest $\delta^{18}O$ values (~+12 ‰) form a tight cluster in Ca# (0.14–0.18) (Fig. 7b). Except for garnet 138-7-3, all garnets follow the trend (R^2 = 0.77; n = 15) of increasing Cr# (molar 100×Cr/(Cr+Al)) with decreasing $\delta^{18}O$ values. The mildly majoritic garnet 140-2-1 has the highest Cr# and lowest $\delta^{18}O$ along this trend (Fig. 7c).

4. Discussion

4.1. Origin of Koidu eclogites

Three garnet inclusions (Fig. 4a) with negative Eu anomalies indicate that the protoliths of their host eclogites formed from Eu-depleted residual melts as a result of preceding fractionation of plagioclase. The high $\delta^{18}O$ values in these three samples, and almost all other analyzed garnet inclusions (+9.9 to +12.1 ‰; Fig. 5), suggest that their protoliths underwent high degrees of submarine weathering at low temperatures (Muehlenbachs and Clayton, 1972b; Alt et al., 1986; McCulloch et al., 1981). Alteration must have occurred close to the basalt-seawater interface, as $\delta^{18}O$ values > +8 ‰ are restricted to altered oceanic crust (AOC) at depths < 300 m (pillow lavas) (Korolev et al., 2018).

The garnet (140-2-1) with a minor majorite component has a $\delta^{18}O$ value (+6.3 ‰) that is elevated relative to the mantle range but low compared to other eclogitic garnet inclusions from Koidu. The protolith of this garnet may have been situated slightly deeper in the oceanic crust (e.g., lower portion of the volcanic section), where the water/rock ratio was lower and the alteration temperature was

higher, compared to the uppermost portion of the oceanic crust (McCulloch et al., 1981; Alt et al., 1986; Gao et al., 2012). This portion of the oceanic crust then carried the mildly ^{18}O-enriched signature and subducted through the asthenosphere where pyroxene started dissolving into the garnet structure to form majoritic garnet (Akaogi and Akimoto, 1979; Irifune et al., 1986; Moore and Gurney, 1985). The slightly enriched LREE and depleted HREE contents in this garnet (Fig. 4b) are consistent with an increasing compatibility of LREE and a decreasing compatibility of HREE in garnet as the depth increases (Stachel and Harris, 1997). Alternatively, the relatively low $\delta^{18}O$ value and relatively high Cr# in garnet 140-2-1 can be explained by slab-mantle interaction, which will be discussed in the following section.

Positive Eu anomalies and low ∑HREE of garnets in diamond 138-7 are consistent with plagioclase accumulation and, consequently, a protolith that originated as cumulate gabbro within the deep oceanic crust (Salisbury and Christensen, 1978; Jacob, 2004; Aulbach and Jacob, 2016). A mantle-like $\delta^{18}O$ value (+5.4 ‰) indicates a protolith that was located either too deep in the oceanic crust to be altered by seawater (Alt and Teagle, 2000), or from the intermediate depth zone where the temperature of alteration generates mantle-like $\delta^{18}O$ signatures (Schmickler et al., 2004).

4.2. Slab-mantle interaction during diamond formation

Based on their low Cr_2O_3 contents (< 1 wt%; Grütter et al., 2004), all garnet inclusions in this study are classified as eclogitic. It has recently been demonstrated that most majoritic garnets included in diamonds belong to neither a pure eclogitic nor a peridotitic paragenesis, but are intermediate between the two (Kiseeva et al., 2013). An approach based on major element substitutions can better differentiate the parageneses of majoritic garnets, in which peridotitic and pyroxenitic garnets follow the peridotitic majoritic substitution: $2Al^{3+} = Si^{4+} + M^{2+}$, while eclogitic garnets follow the eclogitic majoritic substitution: $M^{2+} + Al^{3+} = Na^{+} + Si^{4+}$, with increasing pressure (Kiseeva et al., 2013). Garnet 140-2-1

follows the trend of peridotitic-pyroxenitic majoritic substitution (Fig. S1). Given its high Mg# (79.0) and elevated Cr# (0.90) relative to the other samples (Table 1) and its low CaO content (4.24 wt%), this combined evidence suggests derivation from a pyroxenitic lithology.

Formation of pyroxenitic inclusions in diamond likely results from the interaction between slab-derived melts and ambient mantle peridotite (Aulbach et al., 2002; Kiseeva et al., 2016). This process is especially prominent in the sublithospheric mantle, as observed from the high abundance of pyroxenitic majoritic garnets (Kiseeva et al., 2013; Regier et al., 2020). This observation was related to a deep depression in the solidus of carbonated oceanic crust, which intersects most slab geotherms and facilitates slab melting at a depth of ~300–700 km (Thomson et al., 2016a). Carbonatite melts derived from subducting slabs can readily migrate into ambient mantle peridotite because of their low dihedral angle with olivine and low viscosity, resulting in efficient elemental and isotopic exchange between melt and mantle (Minarik and Watson, 1995; Hammouda and Laporte, 2000; Walter et al., 2008; Thomson et al., 2016b). Thus, the relatively low $\delta^{18}O$ value (+6.3 ‰), and high Mg# and Cr# in garnet 140-2-1 (Fig. 7) likely are a consequence of diamond crystallization during carbonatite-mantle peridotite interaction. Indeed, at the pressure of formation of this majoritic garnet (~8 GPa), ambient mantle is expected to be very reducing, with a calculated oxygen fugacity (fO_2) close to the iron-wüstite (IW) buffer (Frost and McCammon, 2008). Reduction of carbonates from oxidizing slab-derived melt by the reducing metal-saturated ambient mantle is the likely mechanism of diamond formation in this scenario (Rohrbach and Schmidt, 2011).

The crude correlations between major element compositions and $\delta^{18}O$ for a subset of garnet inclusions in this study (Fig. 7) may be a consequence of seawater alteration in different stratigraphic levels of oceanic crust (Gregory and Taylor, 1981; Aulbach and Jacob, 2016), or kimberlite-like ultramafic metasomatism (Aulbach et al., 2020). Alternatively, these covariations could be associated

with elemental and isotopic exchange between eclogitic diamond substrates and surrounding peridotitic lithospheric mantle facilitated by melts (e.g., Smart et al., 2009). In this case, the cluster of garnet inclusions with low Cr# (0.07–0.15) and the highest $\delta^{18}O$ values (~+12 ‰) may represent the initial compositions of the eclogites, without significant chemical exchange with ambient mantle (Fig. 7). Other garnet inclusions that follow the trends of increasing Mg# and Cr# and decreasing Ca# with decreasing $\delta^{18}O$ could then be explained by various degrees of interaction with surrounding peridotites, in which inward transport of peridotitic components into eclogite was facilitated by eclogite-derived melts, and the extent of chemical exchange depends on the distance from the eclogite-peridotite interface (Smart et al., 2009). Trace element partitioning between garnet and pyroxene was likely affected by this interaction, as the three garnets (138-3-1, 138-5-1 and 138-11-1) with an obvious positive correlation between Ca# and $\delta^{18}O$ also show decreasing LREE contents with decreasing Ca# (Fig. 4b and 7b). The difference in LREE contents could be attributed to crystal-chemical effects, where LREE preferentially partition into garnets with higher Ca# (Harte and Kirkley, 1997; Aulbach et al., 2017).

Garnet 138-7-3 has a mantle-like $\delta^{18}O$ value (+5.4 ‰) and high Ca# (49.7) (Fig. 7b) typical for a cumulate gabbro protolith (e.g., MacGregor and Manton, 1986; Schulze et al., 2000). This garnet originated from deeper layers within oceanic crust that do not show a signature of slab-mantle interaction, implying that its host diamond likely formed during introduction of external carbon, e.g., through asthenosphere-derived fluids/melts (Lai et al., 2022). Alternatively, this diamond may have formed as a result of deserpentinization of altered peridotite in the slab within the diamond stability field, where fluids produced from deserpentinization have mantle-like $\delta^{18}O$. Deserpentinization fluids can be either oxidizing or reducing (Debret and Sverjensky, 2017; Piccoli et al., 2019). Depending on the redox states of both the overlying crustal portion and the deserpentinization fluids, diamonds can form from

reduction of CO_2 or CO_3^{2-}, or oxidation of CH_4. Mixing of deserpentinization fluids of different redox states within the slab may also facilitate precipitation of diamonds (Aulbach et al., 2012; Stachel et al., 2022).

4.3. Variation of $\delta^{18}O$–$\delta^{13}C$: mixing between AOC- and mantle-derived carbon?

Coupled $\delta^{18}O$–$\delta^{13}C$ measurements of garnet-bearing diamonds worldwide (Argyle, Schulze et al., 2013; Damtshaa, Ickert et al., 2013; Siberian placers, Zedgenizov et al., 2016; Finsch, Lowry et al., 1999; Jagersfontein, Ickert et al., 2015; Collier and Juina, Burnham et al., 2015) exhibit a negative "correlation", where garnets with $\delta^{18}O$ near the mantle value are associated with mantle-like carbon ($\delta^{13}C$ = -5 ± 3 ‰; Cartigny et al., 2014), whilst distinctly ^{18}O-enriched garnets have ^{13}C-depleted host diamonds (Fig. 8). Accordingly, diamonds and their garnet inclusions falling along a trend between these two end-members could be interpreted as mixing products between mantle ($\delta^{13}C \approx$ -5 ‰; $\delta^{18}O \approx$ +5.5 ‰) and AOC ($\delta^{13}C \approx$ -30 ‰; $\delta^{18}O \approx$ +12 ‰) reservoirs, with variable $(O/C)_{Mantle}/(O/C)_{AOC}$ ratios controlling the curvature of different mixing arrays.

However, instead of following a full mixing array, Koidu diamonds and their garnet inclusions lie at opposite ends of the supposed trend, where the majority of samples form a cluster with $\delta^{18}O \geq$ +9.9 ‰ and $\delta^{13}C \leq$ -19.4 ‰ (Fig. 8 and Table 3). Since there is no known mantle process that can cause such large ^{18}O enrichment and ^{13}C depletion, this main cluster of Koidu samples represents formation of diamonds and their garnet inclusions in a common surface-derived substrate, with diamond carbon and garnet oxygen both being sourced from uppermost AOC (Ickert et al., 2013) containing biogenic carbonate ± organic matter (Milledge et al., 1983; Kirkley et al., 1991; Li et al., 2019). This tight clustering suggests that with respect to oxygen and carbon, the contribution of a mantle-derived component, if present at all, was minor. In subtle contrast, the observed negative correlation between Cr# and $\delta^{18}O$ of garnets spanning a $\delta^{18}O$ range of +9.9 to +11.3 ‰ may be attributed to eclogite-

peridotite interaction during diamond formation, where the eclogite-derived component dominates the oxygen isotope signature but the small mantle contribution levers the $\delta^{18}O$ value downwards (Fig. 7c). In this scenario, the associated dilution of AOC-derived carbon signatures by mantle carbon however, was negligible, due to elevated carbon concentrations in AOC close to the seawater interface relative to carbon-poor ambient mantle. The very low and varied $\delta^{13}C$ values of the host diamonds from this cluster (-29.6 to -19.4 ‰) thus directly reflect the variable carbon isotope composition of subducted AOC, with e.g., biogenic carbonate having $\delta^{13}C$ as low as -24 ‰ (Li et al., 2019) and organic matter having $\delta^{13}C$ of -26 ± 7 ‰ (Schidlowski, 2001). Possible devolatilization of carbonate from AOC during subduction may decrease $\delta^{13}C$ values further (Shieh and Taylor, 1969; Li et al., 2019). Although four of the Koidu diamonds containing high $\delta^{18}O$ garnets (138-5, 138-9, 143-2 and 146-2) have rim zones with mantle-like $\delta^{13}C$ values (Fig. 8), the garnet inclusions were all located in the centres of the diamonds and thus are not related to the rim zones. The abrupt changes in diamond carbon isotope composition from cores (-26.5 to -24.0 ‰) to rims (-7.0 to -6.0 ‰) document distinct stages of diamond formation involving carbon from difference sources, with the rim zones being precipitated from mantle-derived fluids/melts (Lai et al., 2022).

In contrast to the input of AOC-derived carbon and oxygen required for some Koidu garnet-diamond associations, the mantle-like $\delta^{13}C$ value (-4.7 ‰) of the diamond hosting garnet 138-7-3 can be explained by a low carbon content in the gabbroic layers of subducting slabs (Li et al., 2019), which requires externally sourced, mantle-derived carbon for the formation of diamonds. However, the scarcity of diamond in eclogites derived from gabbroic layers implies that the available volume of the required mantle-derived fluids/melts was either small or that the redox conditions in the subducted gabbroic substrate were not suitable for diamond formation from the carbon species contained in the mantle-derived fluids/melts.

The host diamond of majoritic garnet 140-2-1 has elevated $\delta^{13}C$ values ranging from -4.2 to 0 ‰ (inner zone: $\delta^{13}C$ = -4.2 ‰; outer zone: $\delta^{13}C$ = -1.8 to 0 ‰; average $\delta^{13}C$ = -2.6 ‰; Fig. 9). Similar mildly ^{13}C-enriched carbon isotope compositions were observed on the West African Craton for majoritic garnet-included diamonds from Kankan ($\delta^{13}C$ = -3.1 to +0.9 ‰) and were attributed to diamond formation from subducted normal marine carbonates (Stachel et al., 2002). As discussed in section 4.2, the majoritic garnet with a $\delta^{18}O$ value of +6.3 ‰ and its ^{13}C-enriched host diamond could have crystallized during the interaction of a slab-derived carbonatitic melt and ambient mantle. The carbon isotope signature of the outer zone of this diamond then may be attributed to predominantly slab-derived carbon (normal marine carbonates; $\delta^{13}C \approx 0$ ‰). The mantle-like $\delta^{13}C$ value in the inner zone could be explained by formation of diamond in the peridotitic substrate from mantle-derived carbon prior to or at the initial stages of infiltration of slab-derived melt. This was followed by crystallization of the overgrowth layer (outer zone) along with the majoritic garnet inclusion during melt-peridotite interaction. The drop in nitrogen concentrations and sharp decrease in cathodoluminescence response from the inner ([N] = 51–84 at.ppm) to the outer zone ([N] = 0.6–0.7 at.ppm) (Fig. 9) of this diamond clearly documents distinct growth episodes.

4.4. Variation of $\delta^{18}O$–$\delta^{15}N$: mixing between AOC- and mantle-derived nitrogen?

Through its mantle-like $\delta^{13}C$ (-4.7 ‰) and $\delta^{15}N$ (-6.9 ‰) values, diamond 138-7, containing a gabbroic garnet inclusion, demonstrates a coupled origin of carbon and nitrogen, likely from asthenosphere-derived fluids/melts (Lai et al., 2022) or from fluids derived from deserpentinization processes (Aulbach et al., 2012). The association of mantle-like $\delta^{15}N$ and $\delta^{18}O$ (+5.4 ‰) values implies that the gabbroic protolith did not significantly interact with hydrothermal fluids during the seafloor alteration stage (Alt and Teagle, 2000), and thus, in the absence of low-temperature clay formation – as invoked, for example by Li et al. (2019) to explain highly positive $\delta^{15}N$ in some diamonds, did not

incorporate significant nitrogen with a characteristic ^{15}N-enriched signature at the site of future diamond formation.

Other host diamonds in this study with nitrogen contents sufficiently high for isotopic analysis have $\delta^{15}N$ values between -5.6 and +1.3 ‰, except for one outlier with $\delta^{15}N$ = +9.9 ‰ (Table 3). The small portion of positive $\delta^{15}N$ values in Koidu diamonds is attributed to a contribution of nitrogen from clay minerals formed by low-temperature (< 100 ºC) alteration of oceanic crust (Busigny et al., 2005; Bebout et al., 2018; Li et al., 2019; Li and Li, 2022). During subduction, devolatilization of nitrogen from AOC further increases $\delta^{15}N$ values in subducted materials (Bebout and Fogel, 1992; Cartigny et al., 2014), resulting in diverse $\delta^{15}N$ values in AOC. Some Koidu diamonds are associated with convecting mantle-like $\delta^{15}N$ values (-5.6 to -2.0 ‰), but with clearly subducted oxygen ($\delta^{18}O$ = +10.3 to +11.8 ‰) and carbon ($\delta^{13}C$ = -26.5 to -22.0 ‰) isotope signatures. This suggests the possibility of independent sources for (1) carbon and oxygen and (2) nitrogen during the diamond-forming process, with carbon and oxygen originating locally from subducted AOC while nitrogen was largely derived from the mantle. This decoupling of carbon and nitrogen isotope signatures is indeed relatively common in diamonds worldwide (Cartigny et al., 2014; Mikhail et al, 2014).

To investigate the extent of mixing of nitrogen derived from AOC and the mantle during diamond precipitation, we model mixing arrays using different oxygen/nitrogen (O/N) ratios of AOC and the mantle (see supplementary information for details of modeling methods). Mixing models involve two major reservoirs as the endmembers: the mantle ($\delta^{15}N$ = -5.0 ‰; $\delta^{18}O$ = +5.5 ‰) and AOC (represented by diamond 131-2 with $\delta^{15}N$ = +9.9 ‰ and $\delta^{18}O$ = +12.1 ‰). Curvature of the mixing arrays is controlled by $n = (O/N)_{AOC}/(O/N)_{mantle}$ ratios. Note that the oxygen contents of eclogite and peridotite are similar (Cartigny et al., 2014), thus the effect of changing oxygen content on the O/N ratio is negligible and the major parameter that controls the curvature of the mixing model is the nitrogen

content of the two interacting reservoirs. Koidu diamonds are best fitted by the mixing curves with n > 1 (e.g., n = 10, 25 and 70 shown in Fig. 10). These mixing curves require a mantle reservoir with higher nitrogen content compared to AOC, indicating that the contribution of nitrogen from the mantle during diamond formation is high (mantle-derived nitrogen > 60%; Fig. 10). This could be explained by diamond formation in eclogitic substrates facilitated by a mantle-derived fluid/melt pulse, in which the mantle-derived fluid/melt carried a comparatively high concentration of nitrogen but negligible carbon, thus adding a mantle-like $\delta^{15}N$ signature to the diamonds without affecting their crustal $\delta^{13}C$ signature. Crustal nitrogen remains stable in slabs as NH^{4+} in potassium-bearing minerals and transfers to the deep mantle only in cold subduction zones; in warm subduction zones, however, there is substantial nitrogen loss during slab devolatilization and, thus, the amount of crustal nitrogen left in the downgoing slab for subsequent diamond formation becomes negligible (Labidi, 2022).

An alternative explanation is provided by observations of oxygen and nitrogen isotope compositions of the altered basaltic sections recovered at Ocean Drilling Program Site 801, which are characterized by high $\delta^{18}O$ (+8.7 to +25.7 ‰; Alt, 2003) and a wide range of $\delta^{15}N$ (-11.6 to +1.2 ‰; Li et al., 2007) values. The isotope compositions of the super-composite (constructed to represent the bulk composition of the upper oceanic crust; Alt, 2003) at Site 801 show mantle-like $\delta^{15}N$ values (-5.4 ‰; Li et al., 2007) with very high $\delta^{18}O$ values (+12.0 ‰; Alt, 2003). This suggests the possibility that mantle-like $\delta^{15}N$ values of some Koidu diamonds may still derive from an AOC source and as such, their nitrogen isotope compositions are not “decoupled” from the carbon and oxygen isotope signatures recorded by the diamond-garnet association at Koidu.

5. Conclusions

The coupled $\delta^{13}C$–$\delta^{15}N$–$\delta^{18}O$ signatures and elemental compositions of diamonds and their eclogitic inclusions from the Koidu mine suggests three possible modes of diamond formation during slab-mantle interaction:

(1) In the gabbroic layer of oceanic crust where the concentration of crustal carbon is low, diamond formation relies on carbon sourced from mantle-derived fluids/melts, thus the single Koidu diamond formed in this layer has mantle-like carbon and nitrogen isotope compositions ($\delta^{13}C$ = -4.7 ‰; $\delta^{15}N$ = -6.9 ‰). The protolith of this diamond substrate was not significantly altered by seawater and consequently, the gabbroic garnet inclusion has an unperturbed oxygen isotope composition ($\delta^{18}O$ = +5.4 ‰).

(2) In the uppermost basaltic layer of altered oceanic crust, the concentration of carbon is high and dominates the carbon budget for diamond formation. Diamonds with strongly ^{13}C-depleted carbon isotope compositions ($\delta^{13}C$ = -29.6 to -19.4 ‰) document carbon derived from biogenic carbonate and/or organic matter, with a negligible contribution of normal marine carbonates. Nitrogen isotope compositions of this diamond population fall in an only mildly ^{15}N enriched range between -5.6 and +1.3 ‰ (one outlier at +9.9 ‰). This suggests that either the nitrogen budget during diamond formation was dominated by mantle-derived nitrogen, arriving from an external, mantle-hosted fluid source, or the subducted AOC substrate for Koidu diamonds had an unusual nitrogen isotope composition (without ^{15}N enrichment), similar to that observed in oceanic crust at ODP site 801. The basaltic protoliths that formed the host eclogites to this suite of diamonds were intensely altered by seawater at low temperatures prior to subduction, imparting strongly ^{18}O-enriched isotopic compositions ($\delta^{18}O$ = +9.9 to +12.1 ‰) on garnet inclusions derived from this layer. If not related to stratigraphic position of the protoliths within the upper oceanic crust or kimberlite-like ultramafic metasomatism, covariations between major

element and oxygen isotope compositions of garnet inclusions suggest chemical exchange between eclogite and ambient mantle peridotite coeval with diamond formation. This exchange may have been facilitated by melt generated during partial melting of eclogite, in which the degree of chemical exchange depends on the distance of garnets from the eclogite-peridotite interface, i.e., the distance of melt-assisted inward diffusion of elements from peridotite.

(3) One Koidu diamond containing a mildly majoritic garnet inclusion indicates that slab-derived fluids/melts infiltrated ambient mantle peridotite and precipitated pyroxenitic diamonds. The core and rim structure of the precipitated diamond suggests that the core formed from predominantly mantle-derived carbon (core zone $\delta^{13}C$ = -4.2 ‰) and the rim from slab-derived crustal carbon (rim zone $\delta^{13}C$ = -1.8 to 0 ‰). Peridotite can efficiently buffer the oxygen isotope composition of infiltrating slab-derived fluids/melts, driving the $\delta^{18}O$ value of the garnet inclusion (+6.3 ‰) towards the mantle range compared with the much higher values observed in other garnets within Koidu diamonds. The high Mg#, elevated Cr# and low Ca# of the garnet inclusion are all consistent with a high degree of buffering of slab-derived components during interaction with the mantle.

Acknowledgments

MYL acknowledges support through a NSERC CREATE (DERTS) funding. TS and DGP acknowledge support through NSERC Discovery grants. We thank Andrew Locock and Yan Luo for help with EPMA and LA-ICP-MS, respectively, and Robert Dokken for mount preparation and imaging for SIMS analyses. We thank reviewers for thorough reviews and constructive comments, as well as Anne Peslier for efficient editorial handling.

Appendix A. Supplementary Material

Details of SIMS analysis and mixing model are provided in the methodology section in supplementary material. Oxygen isotope compositions for all analyzed spots are shown in Table S1. Trends of peridotitic-pyroxenitic and eclogitic majoritic substitution are shown in Fig. S1.

References

Ackerson M. R., Watson E. B., Tailby N. D. and Spear F. S. (2017) Experimental investigation into the substitution mechanisms and solubility of Ti in garnet. *Am. Mineral.* **102**, 158–172.

Akaogi M. and Akimoto S. (1979) High-pressure phase equilibria in a garnet lherzolite, with special reference to Mg^{2+} - Fe^{2+} partitioning among constituent minerals. *Phys. Earth Planet. Inter.* **19**, 31–51.

Akizuki M. (1989) Growth structure and crystal symmetry of grossular garnets from the Jeffrey mine, Asbestos, Quebec, Canada. *Am. Mineral.* **74**, 859–864.

Alt J. C. (2003) Stable isotopic composition of upper oceanic crust formed at a fast spreading ridge, ODP Site 801. *Geochem. Geophys.* **4**, 1–11.

Alt J. C. and Teagle D. A. H. (2000) Hydrothermal alteration and fluid fluxes in ophiolites and oceanic crust. *Geol. Soc. Am. Spec. Pap.* **349**, 273–282.

Alt J. C., Muehlenbachs K. and Honnorez J. (1986) An oxygen isotopic profile through the upper kilometer of the oceanic crust, DSDP Hole 504B. *Earth Planet. Sci. Lett.* **80**, 217–229.

Aulbach S. (2020) Temperature-dependent rutile solubility in garnet and clinopyroxene from mantle eclogite: implications for continental crust formation and V-based oxybarometry. *J Petrol.* **61**, egaa065.

Aulbach S. and Jacob D. E. (2016) Major- and trace-elements in cratonic mantle eclogites and pyroxenites reveal heterogeneous sources and metamorphic processing of low-pressure protoliths. *Lithos* **262**, 586–605.

Aulbach S. and Arndt N. T. (2019) Origin of high-Mg bimineralic eclogite xenoliths in kimberlite – reply to comment from Claude Herzberg. *Earth Planet. Sci. Lett.* **510**, 234–237.

Aulbach S., Stachel T., Viljoen K. S., Brey G. P. and Harris J. W. (2002) Eclogitic and websteritic diamond sources beneath the Limpopo Belt - Is slab-melting the link? *Contrib. to Mineral. Petrol.* **143**, 56–70.

Aulbach S., Stachel T., Heaman L. M. and Carlson J. A. (2011) Microxenoliths from the Slave craton: archives of diamond formation along fluid conduits. *Lithos* **126**, 419-434.

Aulbach S., Stachel T., Seitz H. M. and Brey G. P. (2012) Chalcophile and siderophile elements in sulphide inclusions in eclogitic diamonds and metal cycling in a Paleoproterozoic subduction zone. *Geochim. Cosmochim. Acta* **93**, 278–299.

Aulbach S., Jacob D. E., Cartigny P., Stern R. A., Simonetti S. S., Wörner G. and Viljoen K. S. (2017) Eclogite xenoliths from Orapa: ocean crust recycling, mantle metasomatism and carbon cycling at the western Zimbabwe craton margin. *Geochim. Cosmochim. Acta* **213**, 574–592.

Aulbach S., Massuyeau M., Garber J. M., Gerdes A., Heaman L. M. and Viljoen K. S. (2020) Ultramafic carbonated melt- and auto- metasomatism in mantle eclogites: compositional effects and

geophysical consequences. *Geochem. Geophys.* **21**, e2019GC008774.

Baertschi P. (1976) Absolute ^{18}O content of standard mean ocean water. *Earth Planet. Sci. Lett.* **31**, 341–344.

Barth M. G., Rudnick R. L., Horn I., McDonough W. F., Spicuzza M. J., Valley J. W. and Haggerty S. E. (2001) Geochemistry of xenolithic eclogites from West Africa, part I: A link between low MgO eclogites and archean crust formation. *Geochim. Cosmochim. Acta* **65**, 1499–1527.

Barth M. G., Rudnick R. L., Horn I., McDonough W. F., Spicuzza M. J., Valley J. W. and Haggerty S. E. (2002) Geochemistry of xenolithic eclogites from West Africa, part 2: Origins of the high MgO eclogites. *Geochim. Cosmochim. Acta* **66**, 4325–4345.

Bartholomé P. (1960) Genesis of the Gore Mountain garnet deposit, New York. *Econ. Geol.* **55**, 255–277.

Bebout G. E. and Fogel M. L. (1992) Nitrogen-isotope compositions of metasedimentary rocks in the Catalina Schist, California: implications for metamorphic devolatilization history. *Geochim. Cosmochim. Acta* **56**, 2839–2849.

Bebout G. E., Banerjee N. R., Izawa M. R. M., Kobayashi K., Lazzeri K., Ranieri L. A. and Nakamura E. (2018) Nitrogen concentrations and isotopic compositions of seafloor-altered terrestrial basaltic glass: implications for astrobiology. *Astrobiology* **18**, 330–342.

Bédard J. H. (1994) A procedure for calculating the equilibrium distribution of trace elements among the minerals of cumulate rocks, and the concentration of trace elements in the coexisting liquids. *Chem. Geol.* **118**, 143–153.

Beyer C. and Frost D. J. (2017) The depth of sub-lithospheric diamond formation and the redistribution

of carbon in the deep mantle. *Earth Planet. Sci. Lett.* **461**, 30–39.

Bishop F. C., Smith J. V. and Dawson J. B. (1976) Na, P, Ti and coordination of Si in garnet from peridotite and eclogite xenoliths. *Nature* **260**, 696–697.

Bishop F. C., Smith J. V. and Dawson J. B. (1978) Na, K, P and Ti in garnet, pyroxene and olivine from peridotite and eclogite xenoliths from African kimberlites. *Lithos* **11**, 155–173.

Burnham A. D., Thomson A. R., Bulanova G. P., Kohn S. C., Smith C. B. and Walter M. J. (2015) Stable isotope evidence for crustal recycling as recorded by superdeep diamonds. *Earth Planet. Sci. Lett.* **432**, 374–380.

Busigny V., Laverne C. and Bonifacie M. (2005) Nitrogen content and isotopic composition of oceanic crust at a superfast spreading ridge: A profile in altered basalts from ODP Site 1256, Leg 206. *Geochem. Geophys.* **6**, 1–16.

Caporuscio F. A. and Smyth J. R. (1990) Trace element crystal chemistry of mantle eclogites. *Contrib. to Mineral. Petrol.* **105**, 550–561.

Cartigny P., Palot M., Thomassot E. and Harris J. W. (2014) Diamond formation: a stable isotope perspective. *Annu. Rev. Earth Planet. Sci.* **42**, 699–732.

Collerson K. D., Williams Q., Kamber B. S., Omori S., Arai H. and Ohtani E. (2010) Majoritic garnet: a new approach to pressure estimation of shock events in meteorites and the encapsulation of sub-lithospheric inclusions in diamond. *Geochim. Cosmochim. Acta* **74**, 5939–5957.

Debret B. and Sverjensky D. A. (2017) Highly oxidising fluids generated during serpentinite breakdown in subduction zones. *Sci. Rep.* **7**, 1–6.

Deines P. and Harris J. W. (1995) Sulfide inclusion chemistry and carbon isotopes of African diamonds.

Geochim. Cosmochim. Acta **59**, 3173–3188.

Deines P. and Haggerty S. E. (2000) Small-scale oxygen isotope variations and petrochemistry of ultradeep (>300 km) and transition zone xenoliths. *Geochim. Cosmochim. Acta* **64**, 117–131.

Eiler J. M. (2001) Oxygen isotope variations of basaltic lavas and upper mantle rocks. *Rev. Mineral. Geochemistry* **43**, 319–364.

Frost D. J. and McCammon C. A. (2008) The Redox State of earth's mantle. *Annu. Rev. Earth Planet. Sci.* **36**, 389–420.

Fung A. T. and Haggerty S. E. (1995) Petrography and mineral compositions of eclogites from the Koidu Kimberlite Complex, Sierra Leone. *J. Geophys. Res.* **100**.

Gao Y., Vils F., Cooper K. M., Banerjee N., Harris M., Hoefs J., Teagle D. A. H., Casey J. F., Elliott T., Laverne C., Alt J. C. and Muehlenbachs K. (2012) Downhole variation of lithium and oxygen isotopic compositions of oceanic crust at East Pacific Rise, ODP Site 1256. *Geochem. Geophys.* **13**.

Gregory R. T. and Taylor H. P. (1981) An oxygen isotope profile in a section of Cretaceous oceanic crust, Samail ophiolite, Oman: evidence for $\delta^{18}O$ buffering of the oceans by deep (>5 km) seawater-hydrothermal circulation at mid-ocean ridges. *J. Geophys. Res. Solid Earth* **86**, 2737–2755.

Grew E. S., Locock A. J., Mills S. J., Galuskina I. O., Galuskin E. V. and Hålenius U. (2013) IMA report: Nomenclature of the garnet supergroup. *Am. Mineral.* **98**, 785–810.

Grütter H. S., Gurney J. J., Menzies A. H. and Winter F. (2004) An updated classification scheme for mantle-derived garnet, for use by diamond explorers. *Lithos* **77**, 841–857.

Hammouda T. and Laporte D. (2000) Ultrafast mantle impregnation by carbonatite melts. *Geology* **28**,

283–285.

Harder M., Nowicki T. E., Hetman C. M., Freeman L. and Abedu B. (2013) Geology and evaluation of the K2 Kimberlite, Koidu Mine, Sierra Leone, West Africa. *Proc. 10th Int. Kimberl. Conf.*, pp. 191–208.

Harte B. and Kirkley M. B. (1997) Partitioning of trace elements between clinopyroxene and garnet: data from mantle eclogites. *Chem. Geol.* **136**, 1–24.

Helmstaedt H. and Doig R. (1975) Eclogite nodules from kimberlite pipes of the Colorado plateau - samples of subducted Franciscan-type oceanic lithosphere. *Phys. Chem. Earth*, 95–111.

Hills D. V. and Haggerty S. E. (1989) Petrochemistry of eclogites from the Koidu Kimberlite Complex, Sierra Leone. *Contrib. to Mineral. Petrol.* **103**, 397–422.

Ickert R. B., Stachel T., Stern R. A. and Harris J. W. (2013) Diamond from recycled crustal carbon documented by coupled $\delta^{18}O$–$\delta^{13}C$ measurements of diamonds and their inclusions. *Earth Planet. Sci. Lett.* **364**, 85–97.

Ickert R. B., Stachel T., Stern R. A. and Harris J. W. (2015) Extreme ^{18}O-enrichment in majorite constrains a crustal origin of transition zone diamonds. *Geochem. Perspect. Lett.* **1**, 65–74.

Irifune T. (1987) An experimental investigation of the pyroxene-garnet transformation in a pyrolite composition and its bearing on the constitution of the mantle. *Phys. Earth Planet. Inter.* **45**, 324–336.

Irifune T., Sekine T., Ringwood A. E. and Hibberson W. O. (1986) The eclogite-garnetite transformation at high pressure and some geophysical implications. *Earth Planet. Sci. Lett.* **77**, 245–256.

Jacob D. E. (2004) Nature and origin of eclogite xenoliths from kimberlites. *Lithos* **77**, 295–316.

Jacob D., Jagoutz E., Lowry D., Mattey D. and Kudrjavtseva G. (1994) Diamondiferous eclogites from Siberia: remnants of Archean oceanic crust. *Geochim. Cosmochim. Acta* **58**, 5191–5207.

Kirkley M. B., Gurney J. J., Otter M. L., Hill S. J. and Daniels L. R. (1991) The application of C isotope measurements to the identification of the sources of C in diamonds: a review. *Appl. Geochem.* **6**, 477–494.

Kiseeva E. S., Yaxley G. M., Stepanov A. S., Tkalčić H., Litasov K. D. and Kamenetsky V. S. (2013) Metapyroxenite in the mantle transition zone revealed from majorite inclusions in diamonds. *Geology* **41**, 883–886.

Kiseeva E. S., Wood B. J., Ghosh S. and Stachel T. (2016) The pyroxenite-diamond connection. *Geochem. Perspect. Lett.* **2**, 1–9.

Korolev N. M., Melnik A. E., Li X. H. and Skublov S. G. (2018) The oxygen isotope composition of mantle eclogites as a proxy of their origin and evolution: A review. *Earth-Science Rev.* **185**, 288–300.

Labidi J. (2022) The origin of nitrogen in Earth's mantle: constraints from basalts $^{15}N/^{14}N$ and $N_2/^3He$ ratios. *Chem. Geol.* **597**, 120780.

Lai M. Y., Stachel T., Stern R. A., Hardman M. F., Pearson D. G. and Harris J. W. (2022) Formation of mixed paragenesis diamonds during multistage growth – Constraints from in situ $\delta^{13}C$–$\delta^{15}N$–[N] analyses of Koidu diamonds. *Geochim. Cosmochim. Acta* **323**, 20–39.

Li K. and Li L. (2022) Nitrogen enrichments in sheeted dikes and gabbros from DSDP/ODP/IODP Hole 504B and 1256D: insights into nitrogen recycling in Central America and global subduction

zones. *Geochim. Cosmochim. Acta* **335**, 197–210.

Li K., Li L., Pearson D. G. and Stachel T. (2019) Diamond isotope compositions indicate altered igneous oceanic crust dominates deep carbon recycling. *Earth Planet. Sci. Lett.* **516**, 190–201.

Li L., Bebout G. E. and Idleman B. D. (2007) Nitrogen concentration and $\delta^{15}N$ of altered oceanic crust obtained on ODP Legs 129 and 185: insights into alteration-related nitrogen enrichment and the nitrogen subduction budget. *Geochim. Cosmochim. Acta* **71**, 2344–2360.

Locock A. J. (2008) An Excel spreadsheet to recast analyses of garnet into end-member components, and a synopsis of the crystal chemistry of natural silicate garnets. *Comput. Geosci.* **34**, 1769–1780.

Lowry D., Mattey D. P. and Harris J. W. (1999) Oxygen isotope composition of syngenetic inclusions in diamond from the Finsch Mine, RSA. *Geochim. Cosmochim. Acta* **63**, 1825–1836.

MacGregor I. D. and Manton W. I. (1986) Roberts Victor eclogites: ancient oceanic crust. *J. Geophys. Res.* **91**, 14063–14079.

Mattey D., Lowry D. and Macpherson C. (1994) Oxygen isotope composition of mantle peridotite. *Earth Planet. Sci. Lett.* **128**, 231–241.

McCulloch M. T., Gregory R. T., Wasserburg G. J. and Taylor H. P. (1981) Sm-Nd, Rb-Sr, and $^{18}O/^{16}O$ isotopic systematics in an oceanic crustal section: evidence from the Samail ophiolite. *J. Geophys. Res.* **86**, 2721–2735.

McGetchin T. R. and Silver L. T. (1972) A crustal-upper mantle model for the Colorado plateau based on observations of crystalline rock fragments in the Moses Rock Dike. *J. Geophys. Res.* **77**, 7022–7037.

McLennan S. M. (1989) Rare earth elements in sedimentary rocks: influence of provenance and

sedimentary processes. *Rev. Mineral. Geochem.* **21**, 169–200.

Mikhail S., Verchovsky A. B., Howell D., Hutchison M. T., Southworth R., Thomson A. R., Warburton P., Jones A. P. and Milledge H. J. (2014) Constraining the internal variability of the stable isotopes of carbon and nitrogen within mantle diamonds. *Chem. Geol.* **366**, 14–23.

Mikhail S., Rinaldi M., Mare E. R. and Sverjensky D. A. (2021) A genetic metasomatic link between eclogitic and peridotitic diamond inclusions. *Geochem. Perspect. Lett.* **17**, 33–38.

Milledge H. J., Mendelssohn M. J., Seal M., Rouse J. E., Swart P. K. and Pillinger C. T. (1983) Carbon isotopic variation in spectral type II diamonds. *Nature* **303**, 791–792.

Minarik W. G. and Watson E. B. (1995) Interconnectivity of carbonate melt at low melt fraction. *Earth Planet. Sci. Lett.* **133**, 423–437.

Moore R. O. and Gurney J. J. (1985) Pyroxene solid solution in garnets included in diamond. *Nature* **318**, 553–555.

Muehlenbachs K. and Clayton R. N. (1972a) Oxygen isotope geochemistry of submarine greenstones. *Can. J. Earth Sci.* **9**, 471–478.

Muehlenbachs K. and Clayton R. N. (1972b) Oxygen isotope studies of fresh and weathered submarine basalts. *Can. J. Earth Sci.* **9**, 172–184.

O'Hara M. J. and Yoder H. S. (1967) Formation and fractionation of basic magmas at high pressures. *Scottish J. Geol.* **3**, 67–117.

Philpotts J. A. and Schnetzler C. C. (1968) Europium anomalies and the genesis of basalt. *Chem. Geol.* **3**, 5–13.

Piccoli F., Hermann J., Pettke T., Connolly J. A. D., Kempf E. D. and Vieira Duarte J. F. (2019)

Subducting serpentinites release reduced, not oxidized, aqueous fluids. *Sci. Rep.* **9**, 1–7.

Putlitz B., Matthews A. and Valley J. W. (2000) Oxygen and hydrogen isotope study of high-pressure metagabbros and metabasalts (Cyclades, Greece): implications for the subduction of oceanic crust. *Contrib. to Mineral. Petrol.* **138**, 114–126.

Regier M., Miškovic A., Ickert R. B., Pearson D. G., Stachel T., Stern R. A. and Kopylova M. (2018) An oxygen isotope test for the origin of Archean mantle roots. *Geochem. Perspect. Lett.* **9**, 6–10.

Regier M. E., Pearson D. G., Stachel T., Luth R. W., Stern R. A. and Harris J. W. (2020) The lithospheric-to-lower-mantle carbon cycle recorded in superdeep diamonds. *Nature* **585**, 234–238.

Riches A. J. V., Ickert R. B., Pearson D. G., Stern R. A., Jackson S. E., Ishikawa A., Kjarsgaard B. A. and Gurney J. J. (2016) In situ oxygen-isotope, major-, and trace-element constraints on the metasomatic modification and crustal origin of a diamondiferous eclogite from Roberts Victor, Kaapvaal Craton. *Geochim. Cosmochim. Acta* **174**, 345–359.

Ringwood A. and Major A. (1971) Synthesis of majorite and other high pressure garnets and perovskites. *Earth Planet. Sci. Lett.* **12**, 411–418.

Rohrbach A. and Schmidt M. W. (2011) Redox freezing and melting in the Earth's deep mantle resulting from carbon-iron redox coupling. *Nature* **472**, 209–214.

Russell A. K., Kitajima K., Strickland A., Medaris L. G., Schulze D. J. and Valley J. W. (2013) Eclogite-facies fluid infiltration: constraints from $\delta^{18}O$ zoning in garnet. *Contrib. to Mineral. Petrol.* **165**, 103–116.

Salisbury M. H. and Christensen N. I. (1978) The seismic velocity structure of a traverse through the Bay of Islands Ophiolite Complex, Newfoundland, an exposure of oceanic crust and upper mantle.

J. Geophys. Res. **83**, 805–817.

Schidlowski M. (2001) Carbon isotopes as biogeochemical recorders of life over 3.8 Ga of earth history: evolution of a concept. *Precambrian Res.* **106**, 117–134.

Schmickler B., Jacob D. E. and Foley S. F. (2004) Eclogite xenoliths from the Kuruman kimberlites, South Africa: geochemical fingerprinting of deep subduction and cumulate processes. *Lithos* **75**, 173–207.

Schulze D. J. (1989) Constraints on the abundance of eclogite in the upper mantle. *J. Geophys. Res.* **94**, 4205–4212.

Schulze D. J., Valley J. W. and Spicuzza M. J. (2000) Coesite eclogites from the Roberts Victor kimberlite, South Africa. *Lithos* **54**, 23–32.

Schulze D. J., Harte B., Valley J. W. and Channer D. M. D. (2004) Evidence of subduction and crust – mantle mixing from a single diamond. *Lithos* **77**, 349–358.

Schulze D. J., Harte B., Edinburgh ion microprobe facility staff, Page F. Z., Valley J. W., Channer D. M. D. and Jaques A. L. (2013) Anticorrelation between low $\delta^{13}C$ of eclogitic diamonds and high $\delta^{18}O$ of their coesite and and garnet inclusions requires a subduction origin. *Geology* **41**, 455–458.

Shieh Y. N. and Taylor H. P. (1969) Oxygen and carbon isotope studies of contact metamorphism of carbonate rocks. *J. Petrol.* **10**, 307–331.

Skinner E. M. W., Apter D. B., Morelli C. and Smithson N. K. (2004) Kimberlites of the Man craton, West Africa. *Lithos* **76**, 233–259.

Smart K. A., Heaman L. M., Chacko T., Simonetti A., Kopylova M., Mah D. and Daniels D. (2009) The origin of high-MgO diamond eclogites from the Jericho Kimberlite, Canada. *Earth Planet. Sci. Lett.*

284, 527–537.

Smart K. A., Chacko T., Stachel T., Tappe S., Stern R. A., Ickert R. B. and EIMF (2012) Eclogite formation beneath the northern Slave craton constrained by diamond inclusions: oceanic lithosphere origin without a crustal signature. *Earth Planet. Sci. Lett.* **319–320**, 165–177.

Smit K. V., Shirey S. B. and Wang W. (2016) Type Ib diamond formation and preservation in the West African lithospheric mantle: Re–Os age constraints from sulphide inclusions in Zimmi diamonds. *Precambrian Res.* **286**, 152–166.

Stachel T. and Harris J. W. (1997) Diamond precipitation and mantle metasomatism - evidence from the trace element chemistry of silicate inclusions in diamonds from Akwatia, Ghana. *Contrib. to Mineral. Petrol.* **129**, 143–154.

Stachel T., Harris J. W. and Brey G. P. (1998) Rare and unusual mineral inclusions in diamonds from Mwadui, Tanzania. *Contrib. to Mineral. Petrol.* **132**, 34–47.

Stachel T., Harris J., Aulbach S. and Deines P. (2002) Kankan diamonds (Guinea) III: $\delta^{13}C$ and nitrogen characteristics of deep diamonds. *Contrib. to Mineral. Petrol.* **142**, 465–475.

Stachel T., Aulbach S., Brey G. P., Harris J. W., Leost I., Tappert R. and Viljoen K. S. (2004) The trace element composition of silicate inclusions in diamonds: a review. *Lithos* **77**, 1–19.

Stachel T., Aulbach S. and Harris J. W. (2022) Mineral inclusions in lithospheric diamonds. *Rev. Mineral. Geochem.* **87**, 307–391.

Thomson A. R., Walter M. J., Kohn S. C. and Brooker R. A. (2016a) Slab melting as a barrier to deep carbon subduction. *Nature* **529**, 76–79.

Thomson A. R., Kohn S. C., Bulanova G. P., Smith C. B., Araujo D. and Walter M. J. (2016b) Trace

element composition of silicate inclusions in sub-lithospheric diamonds from the Juina-5 kimberlite: evidence for diamond growth from slab melts. *Lithos* **265**, 108–124.

Tompkins L. A. and Haggerty S. E. (1984) The Koidu kimberlite complex, Sierra Leone: geological setting, petrology and mineral chemistry. In *Developments in Petrology*, vol. 11, pp. 83–105

Walter M. J., Bulanova G. P., Armstrong L. S., Keshav S., Blundy J. D., Gudfinnsson G., Lord O. T., Lennie A. R., Clark S. M., Smith C. B. and Gobbo L. (2008) Primary carbonatite melt from deeply subducted oceanic crust. *Nature* **454**, 622–626.

Weill D. F. and Drake M. J. (1973) Europium anomaly in plagioclase feldspar: experimental results and semiquantitative model. *Science* **180**, 1059–1060.

Zedgenizov D., Rubatto D., Shatsky V., Ragozin A. and Kalinina V. (2016) Eclogitic diamonds from variable crustal protoliths in the northeastern Siberian craton: trace elements and coupled $\delta^{13}C$–$\delta^{18}O$ signatures in diamonds and garnet inclusions. *Chem. Geol.* **422**, 46–59.

Zhang R. Y., Zhai S. M., Fei Y. W. and Liou J. G. (2003) Titanium solubility in coexisting garnet and clinopyroxene at very high pressure: The significance of exsolved rutile in garnet. *Earth Planet. Sci. Lett.* **216**, 591–601.

Table 1. Major element compositions (wt%) of garnet inclusions in 16 Koidu diamonds.

Sample	131-2-2	131-5-8	137-1-6	138-2-1	138-3-1	138-4-1	138-5-1	138-6-2
SiO_2	40.53	40.29	40.22	41.02	40.91	40.38	41.26	40.06
TiO_2	0.36	0.36	0.37	0.47	0.36	0.39	0.39	0.24
Al_2O_3	22.68	22.67	21.99	23.08	23.48	22.94	23.27	22.72
Cr_2O_3	0.02	0.05	0.04	0.15	0.07	0.04	0.08	0.11
FeO^{total}	17.98	16.58	18.58	13.52	17.04	18.32	15.27	15.94
NiO	n.d.	n.d.	n.d.	n.d.	n.d.	n.d.	n.d.	0.01
MnO	0.24	0.38	0.26	0.26	0.25	0.24	0.25	0.29
MgO	12.11	10.13	11.27	15.01	13.04	11.60	15.66	12.19
CaO	6.03	9.59	6.22	6.03	5.91	6.23	4.32	7.24
Na_2O	0.17	0.16	0.16	0.17	0.16	0.18	0.13	0.12
Total	100.11	100.23	99.09	99.71	101.22	100.31	100.63	98.92

Sample	138-7-3	138-9-6	138-11-1	138-12-1	140-2-1	143-2-3	144-1-3	146-2-1
SiO_2	41.00	40.70	41.38	40.48	42.56	40.59	40.38	40.56
TiO_2	0.47	0.38	0.48	0.25	0.86	0.29	0.32	0.33
Al_2O_3	22.98	22.38	23.13	22.88	21.09	22.85	22.94	23.38
Cr_2O_3	0.02	0.04	0.17	0.04	0.28	0.05	0.05	0.04
FeO^{total}	8.99	17.57	14.56	16.64	9.79	17.45	18.00	17.41
NiO	n.d.	n.d.	n.d.	n.d.	0.01	n.d.	n.d.	n.d.
MnO	0.16	0.22	0.26	0.41	0.27	0.24	0.23	0.35
MgO	8.47	12.26	16.83	9.00	20.61	12.33	11.67	13.06
CaO	18.55	6.21	3.57	11.08	4.24	6.29	6.58	5.39
Na_2O	0.18	0.16	0.14	0.13	0.13	0.14	0.14	0.14
Total	100.82	99.93	100.52	100.91	99.82	100.23	100.32	100.67

n.d. = not determined.

Table 2. Trace element concentrations (ppm) of garnet inclusions in 16 Koidu diamonds.

Sample	131-2-2	131-5-8	137-1-6	138-2-1	138-3-1	138-4-1	138-5-1	138-6-2
La	0.005	0.010	0.010	0.021	0.023	0.010	0.009	0.009
Ce	0.149	0.339	0.198	0.428	0.392	0.295	0.148	0.091
Pr	0.104	0.227	0.134	0.159	0.123	0.129	0.084	0.070
Nd	1.347	3.115	1.497	1.483	1.392	1.470	1.067	1.316
Sm	3.100	2.914	3.017	2.672	1.976	3.260	1.362	2.311
Eu	2.084	1.118	1.593	1.322	1.120	1.978	0.724	0.977
Gd	8.880	5.080	9.180	6.060	5.840	9.100	4.360	6.000
Tb	1.688	0.967	1.373	1.087	1.164	1.887	1.061	1.002
Dy	11.420	6.810	9.460	7.270	8.030	13.090	8.560	7.360
Ho	2.404	1.504	2.473	1.529	1.635	2.896	1.976	1.875
Er	7.170	4.651	8.300	4.584	4.893	8.860	5.990	6.250
Tm	1.038	0.661	1.015	0.655	0.697	1.255	0.855	0.807
Yb	7.320	4.736	7.050	4.659	4.882	8.640	5.805	5.510
Lu	1.129	0.726	1.093	0.707	0.737	1.337	0.835	0.836

Sample	138-7-3	138-9-6	138-11-1	138-12-1	140-2-1	143-2-3	144-1-3	146-2-1
La	0.062	0.004	0.002	0.022	0.050	0.037	0.007	0.009
Ce	0.559	0.105	0.000	0.812	0.374	0.418	0.291	0.249
Pr	0.213	0.077	0.061	0.623	0.108	0.192	0.239	0.173
Nd	1.910	1.171	0.784	8.000	0.934	2.040	2.378	1.414
Sm	1.314	3.324	1.218	5.620	0.911	2.700	3.254	2.044
Eu	0.617	1.563	0.656	1.931	0.475	1.660	1.579	1.227
Gd	2.240	8.440	3.603	8.570	2.441	7.520	8.280	6.760
Tb	0.321	1.144	0.810	1.571	0.576	1.622	1.176	1.097
Dy	2.138	7.630	6.600	11.250	4.732	11.680	7.850	8.460
Ho	0.540	1.898	1.578	2.477	1.128	2.610	2.048	2.246
Er	1.646	6.240	5.000	7.370	3.634	8.170	6.750	7.850
Tm	0.182	0.775	0.756	1.054	0.535	1.217	0.836	0.988
Yb	1.116	5.420	5.470	7.640	3.835	8.790	6.070	6.980
Lu	0.155	0.810	0.822	1.171	0.593	1.380	0.941	1.109

Table 3. Average $\delta^{18}O$ values and nitrogen concentrations, $\delta^{13}C$ and $\delta^{15}N$ values of garnet inclusions and their host diamonds, respectively.

Sample	$\delta^{18}O_{VSMOW}$ (‰)	2σ (‰)	$\delta^{13}C_{VPDB}$ (‰)	2σ (‰)	$\delta^{15}N_{Air}$ (‰)	2σ (‰)	[N] (at.ppm)	2σ (at.ppm)
131-2-2	12.1	0.3	-19.4	0.1	9.9	2.6	57	2
131-5-8	10.8	0.3	-25.4	0.2	1.1	3.2	41	2
137-1-6	11.8	0.3	-27.9	0.1	0.6	3.5	33	2
138-2-1	11.8	0.3	-28.3	0.1	—	—	21	1
138-3-1	10.8	0.3	-26.8	0.1	-0.2	0.9	552	17
138-4-1	11.8	0.3	-26.3	0.1	-2.6	1.3	267	9
138-5-1 (rim)	10.3	0.3	-7.0	0.1	-5.8	0.8	968	30
138-5-1 (core)			-26.5	0.1	-5.6	1.2	290	10
138-6-2	11.1	0.3	-22.0	0.1	-2.0	2.5	55	2
138-7-3	5.4	0.3	-4.7	0.1	-6.9	1.2	515	16
138-9-6 (rim)	12.0	0.3	-6.9	0.1	-5.5	0.8	1027	31
138-9-6 (core)			-24.0	0.1	0.2	1.8	71	2
138-11-1	9.9	0.3	-29.6	0.1	1.3	1.2	286	10
138-12-1	11.3	0.3	-28.6	0.1	-1.3	0.9	252	8
140-2-1	6.3	0.3	-2.6	0.1	—	—	34	2
143-2-3 (rim)	11.3	0.3	-6.0	0.2	-4.5	0.8	1070	33
143-2-3 (core)			-24.9	0.1	-2.9	1.0	133	4
144-1-3	11.9	0.3	-25.7	0.1	—	—	21	1
146-2-1 (rim)	11.9	0.3	-7.0	0.1	-4.8	0.9	680	21
146-2-1 (core)			-26.2	0.1	—	—	16	1

Figure 1

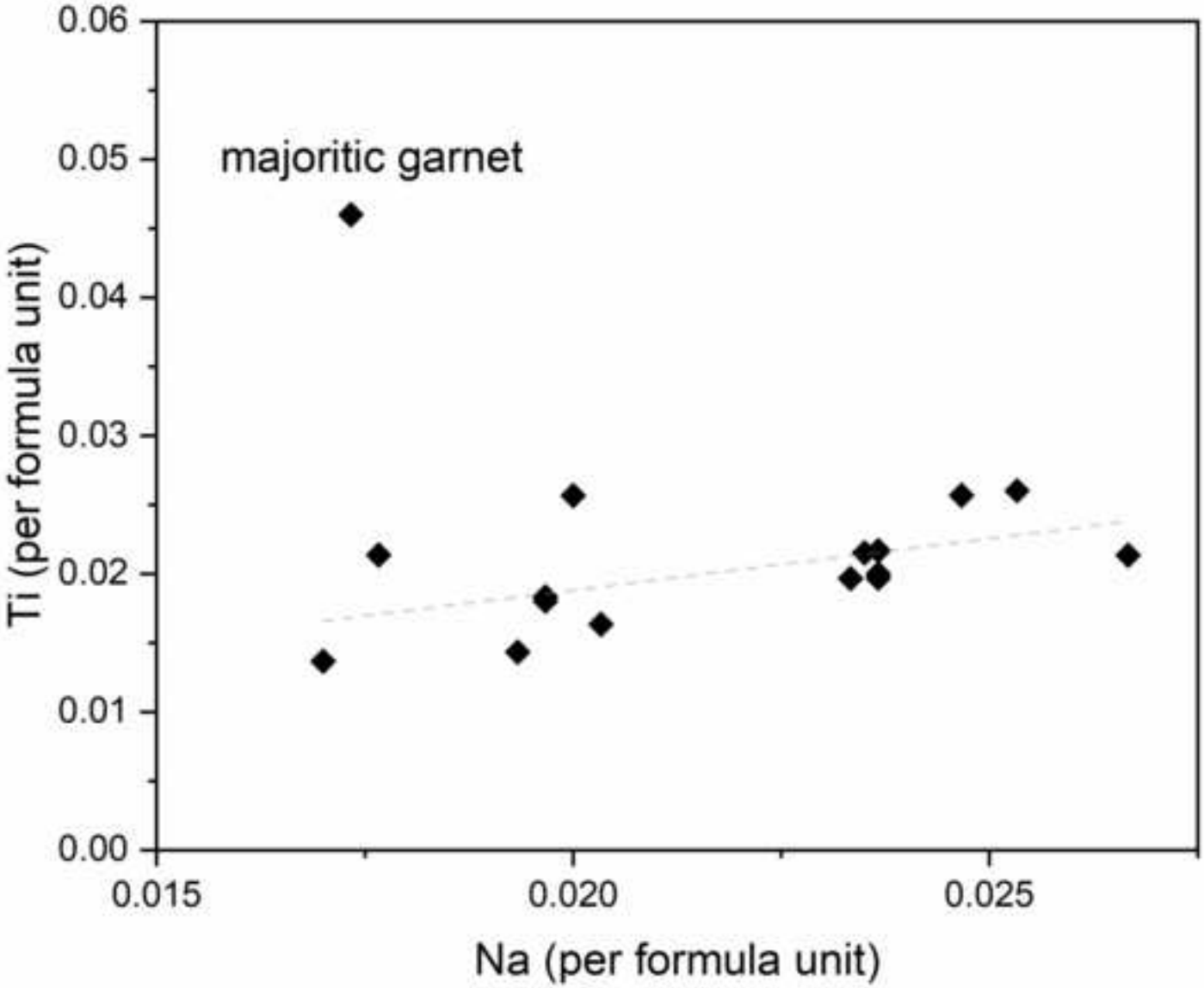

Figure 2

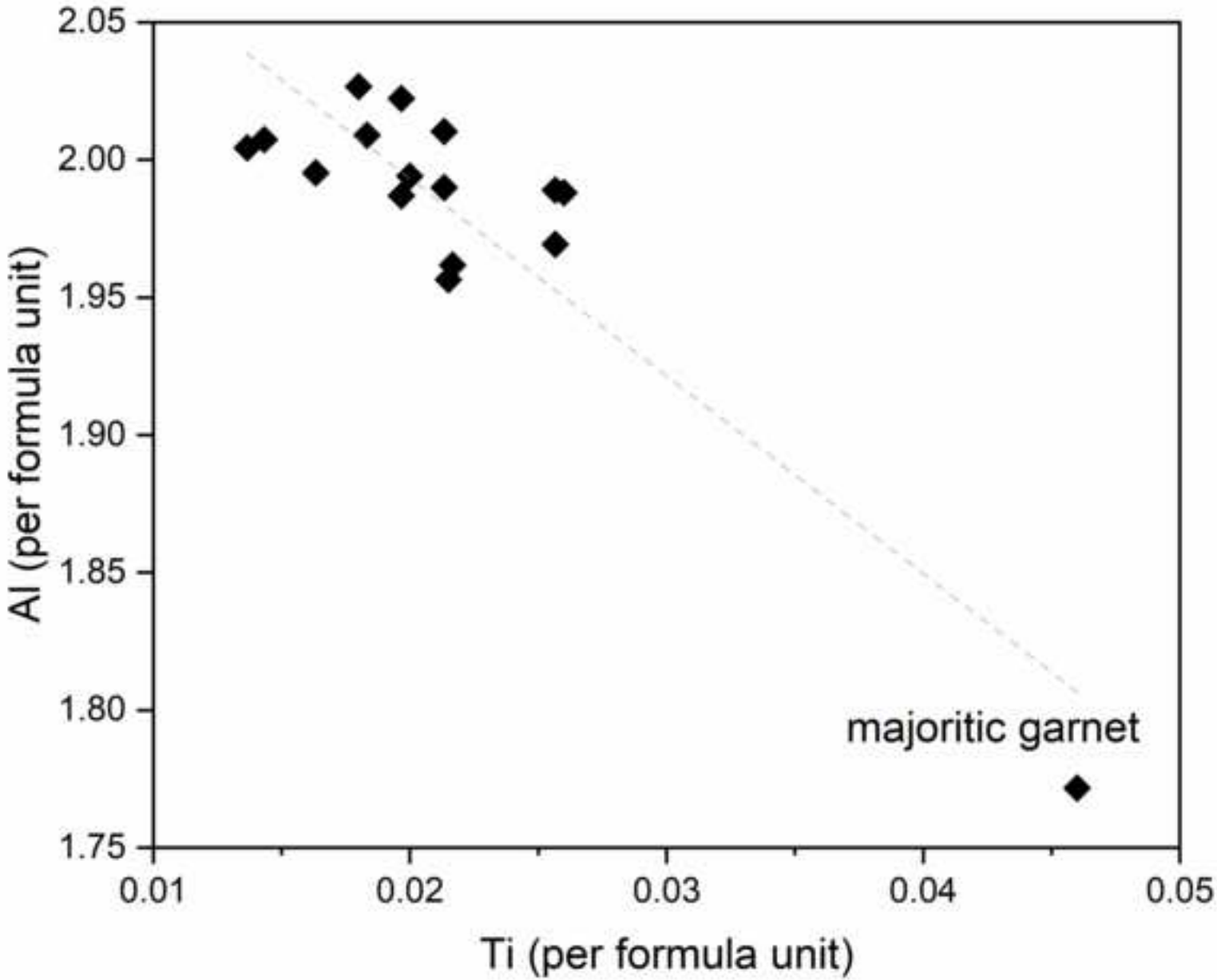

Figure 3

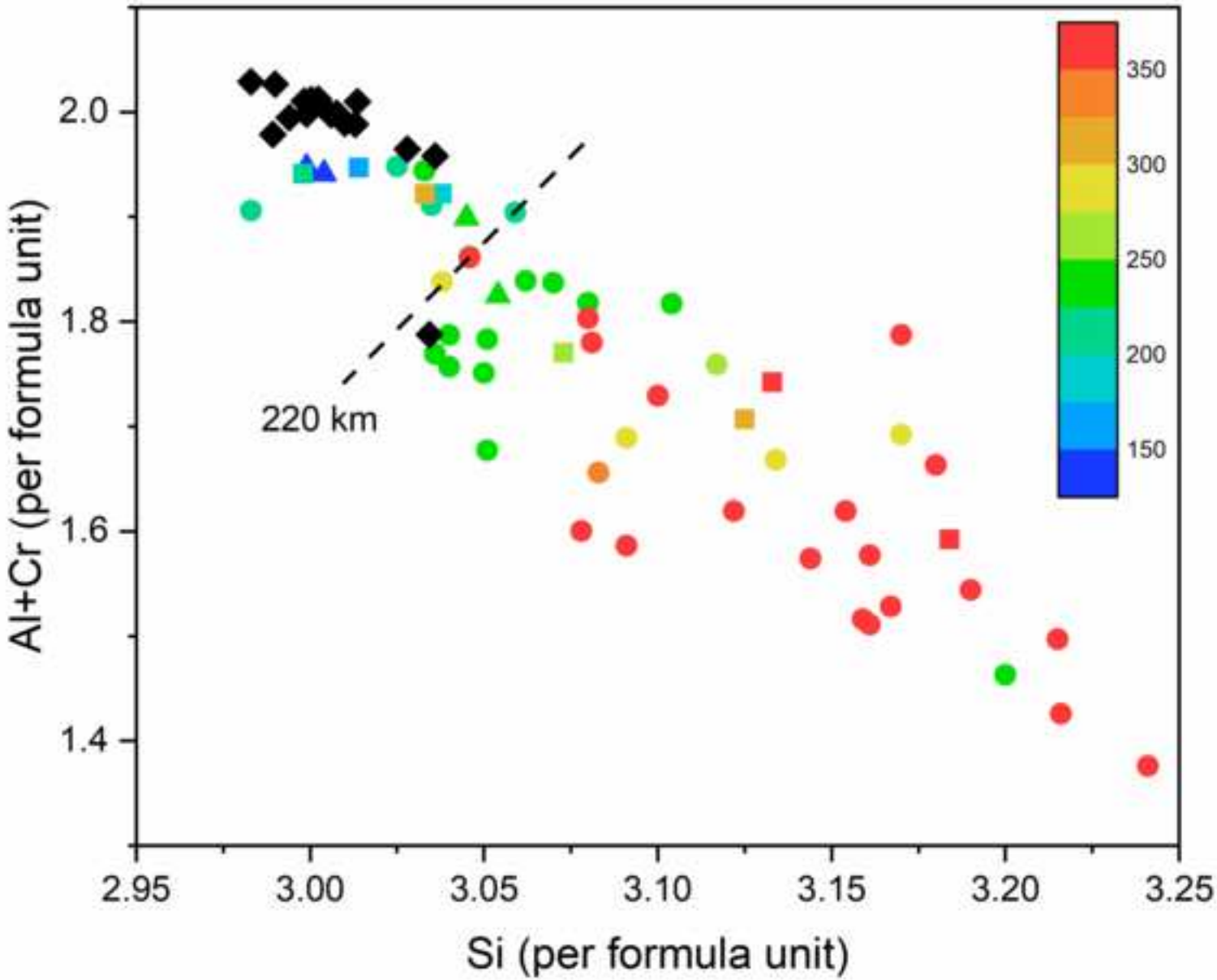

Figure 4a

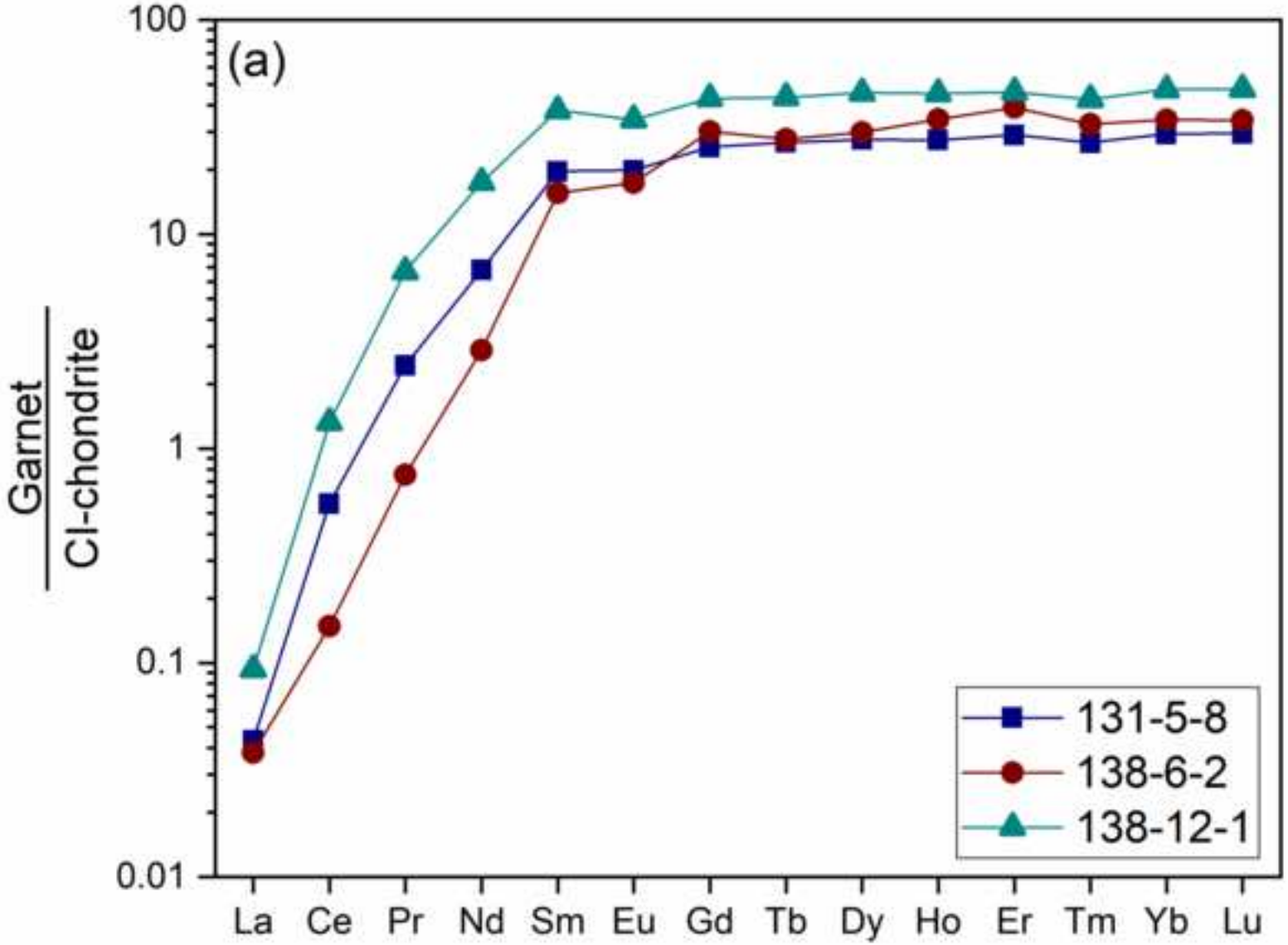

Figure 4b

Click here to access/download;Figure;Figure 4b.tif

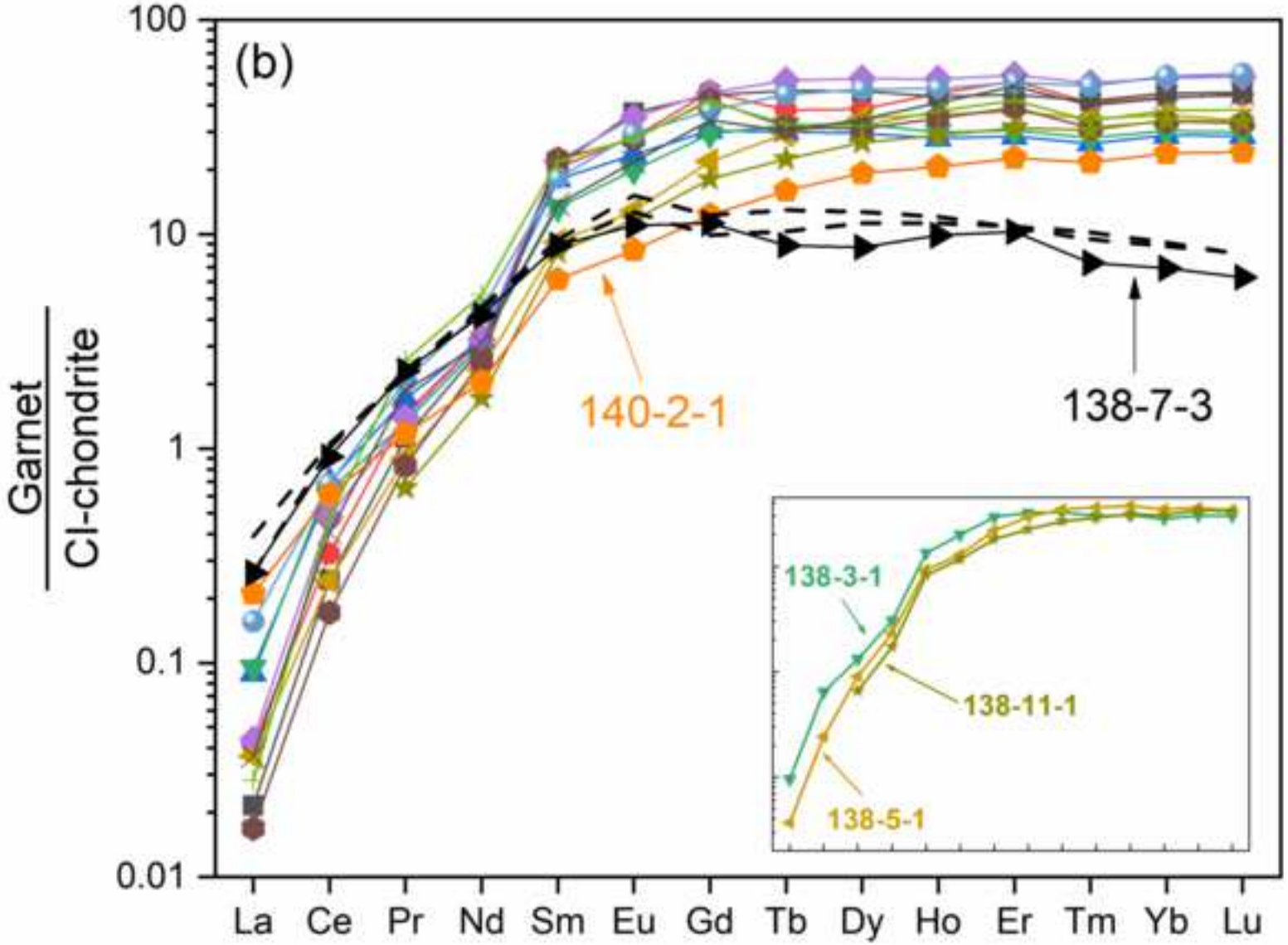

Figure 5

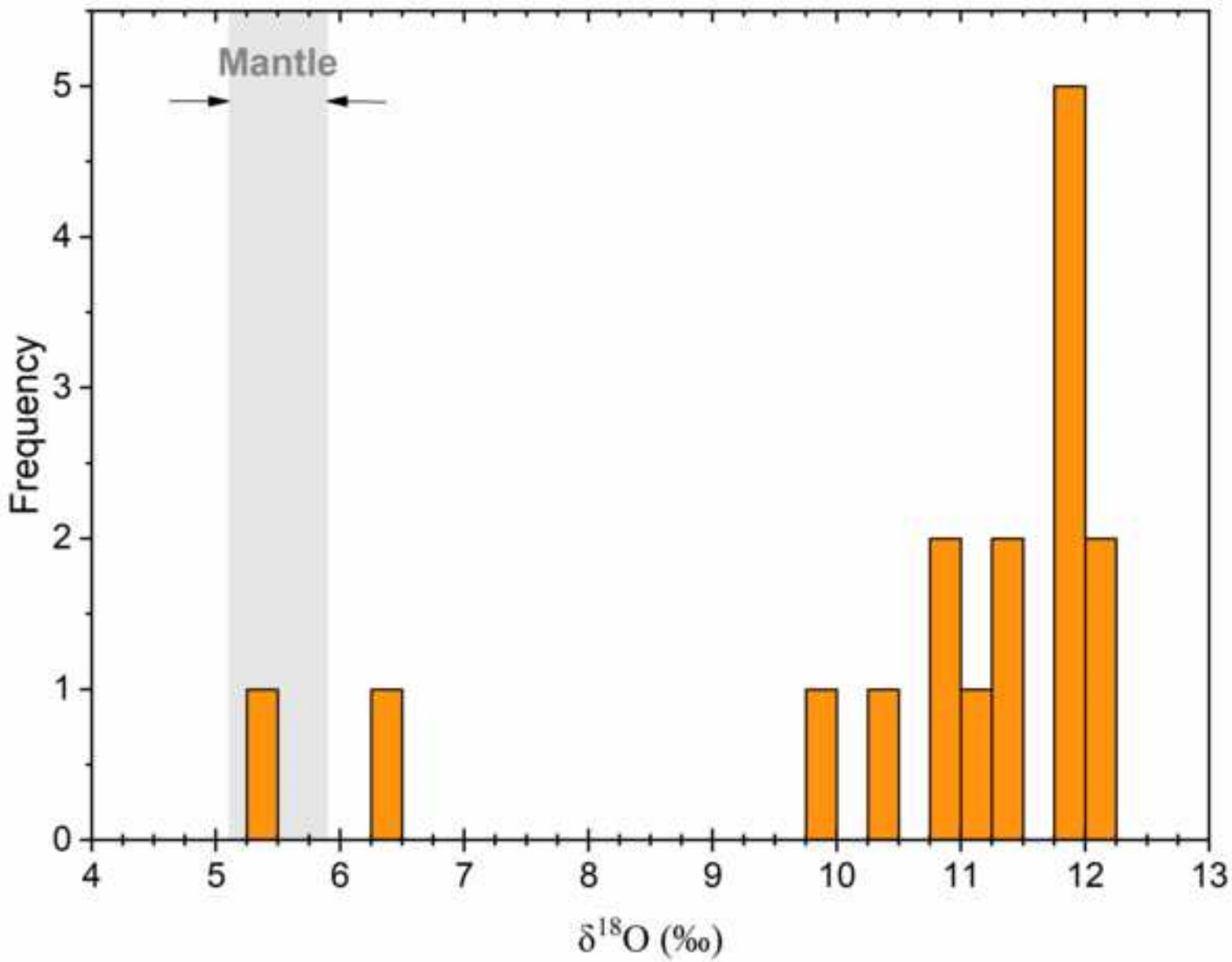

Figure 6

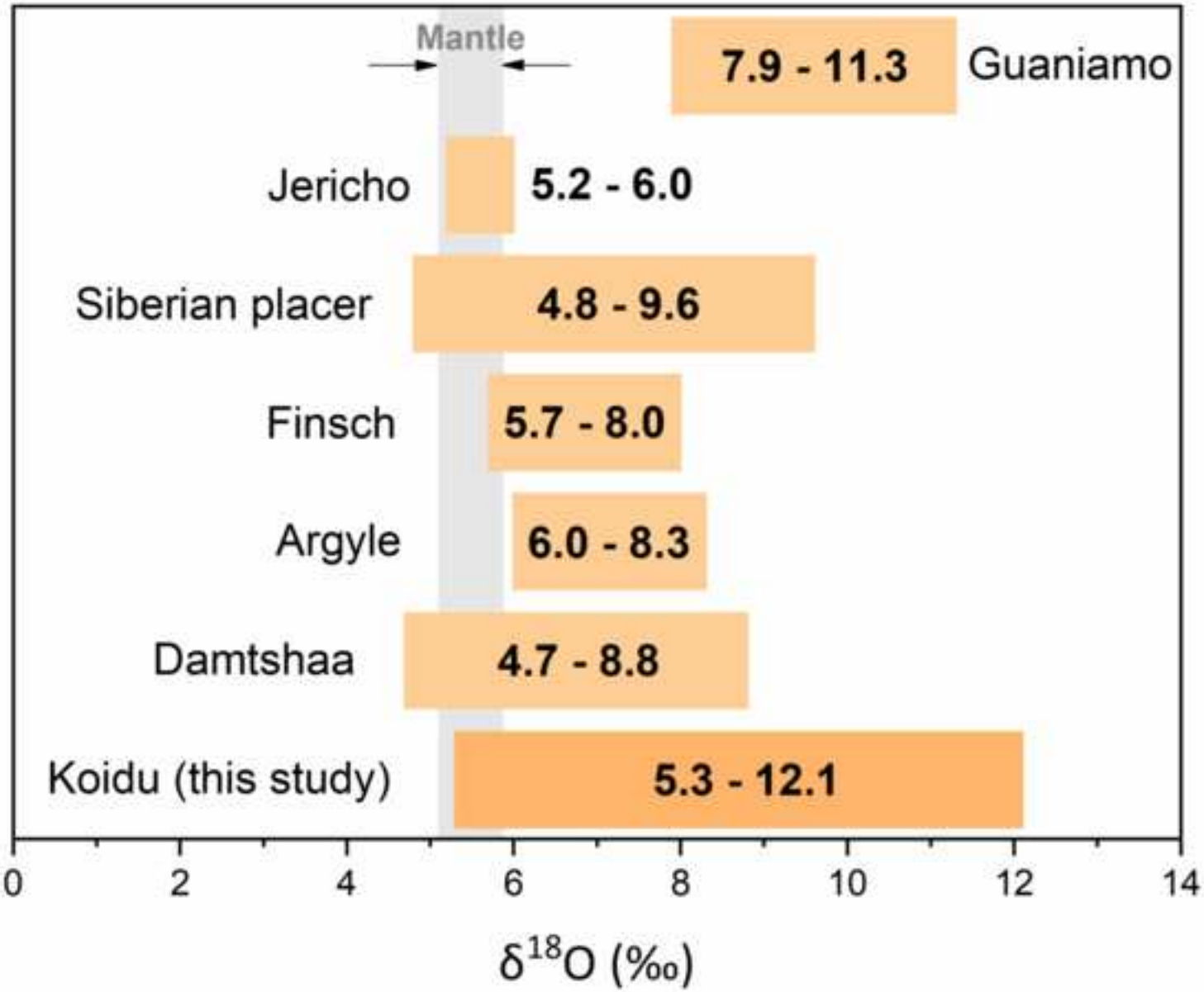

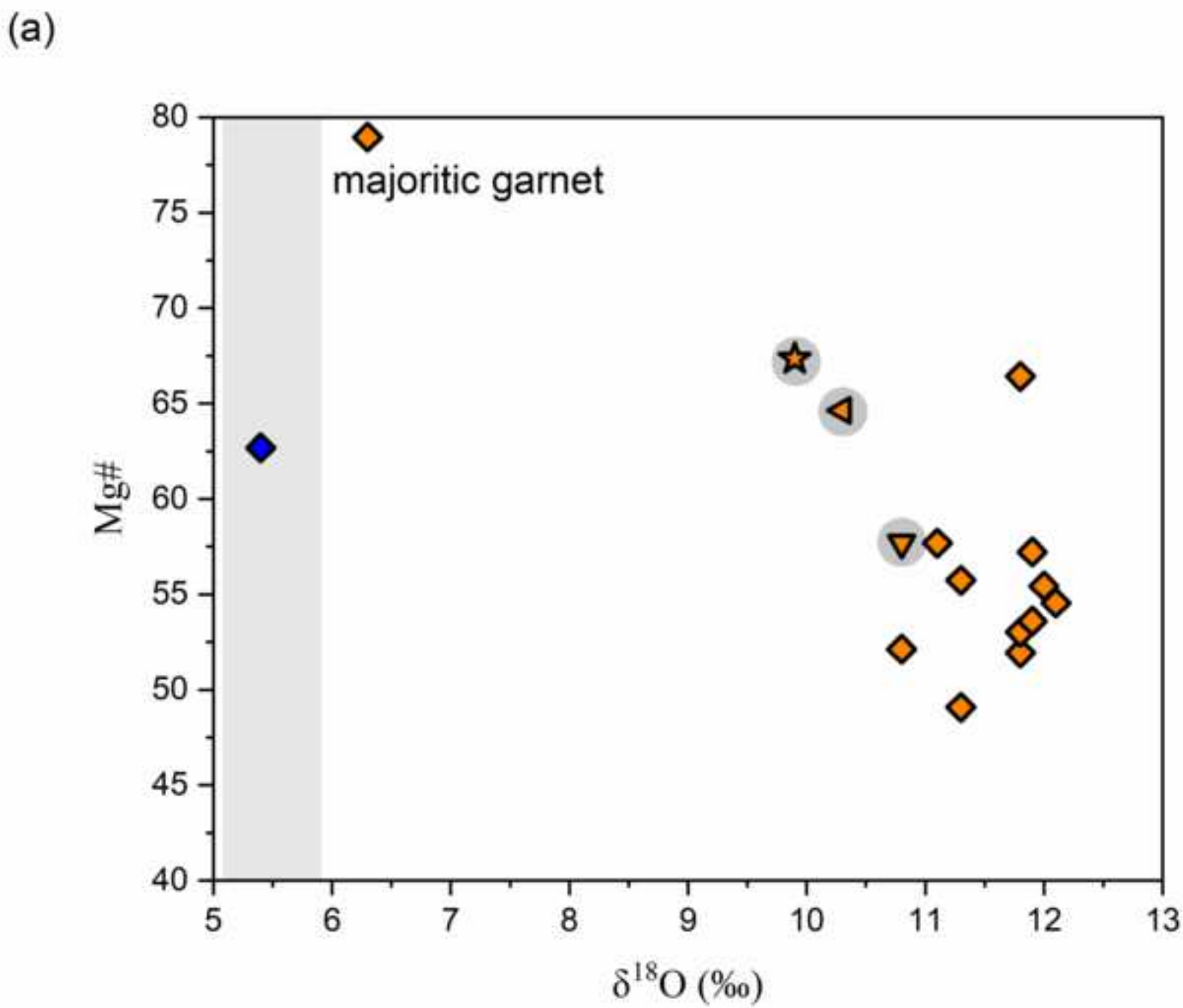

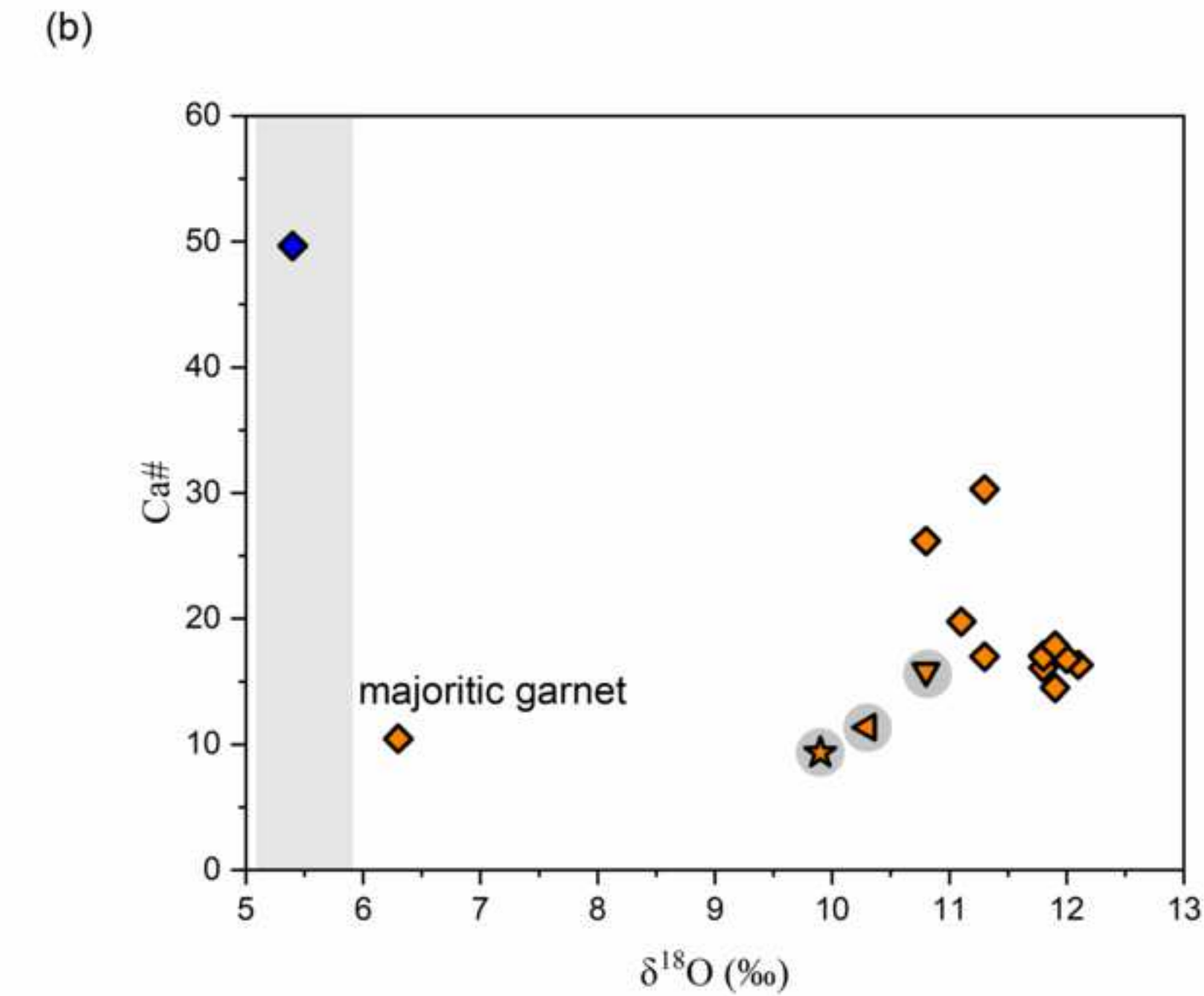

Figure 7c

Click here to access/download;Figure;Figure 7c.tif

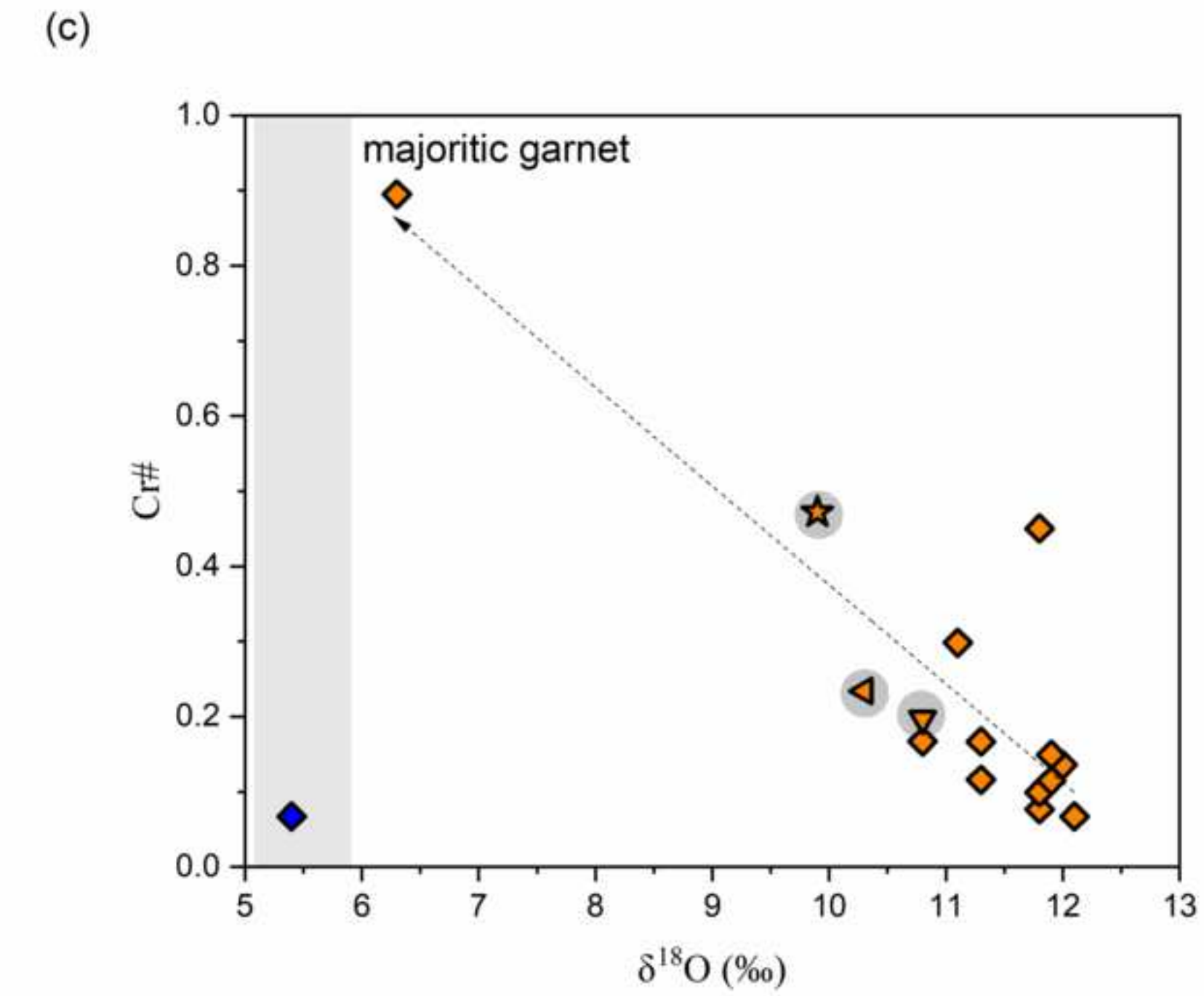

Figure 8

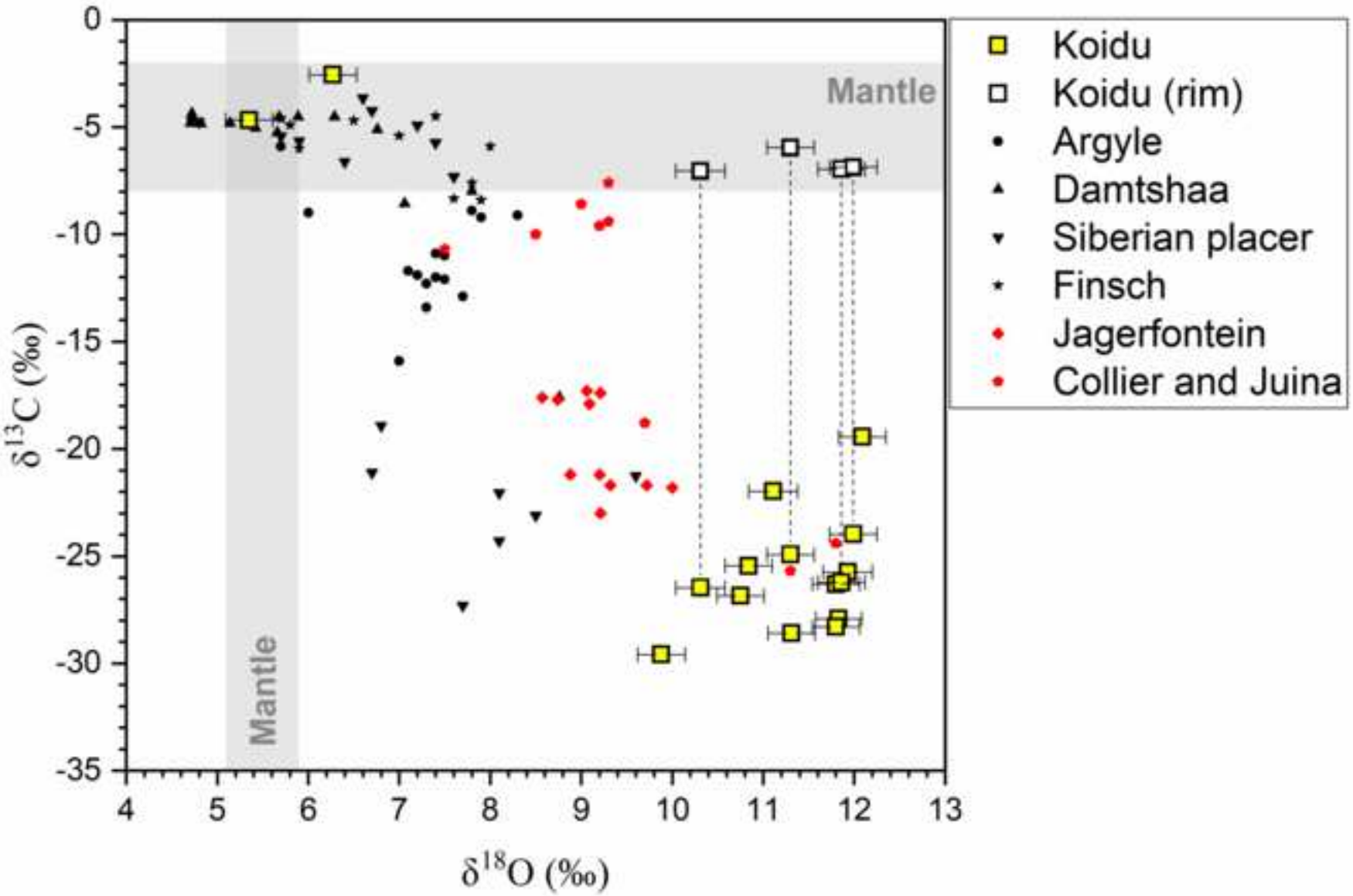

Figure 9

Click here to access/download;Figure;Figure 9.tif

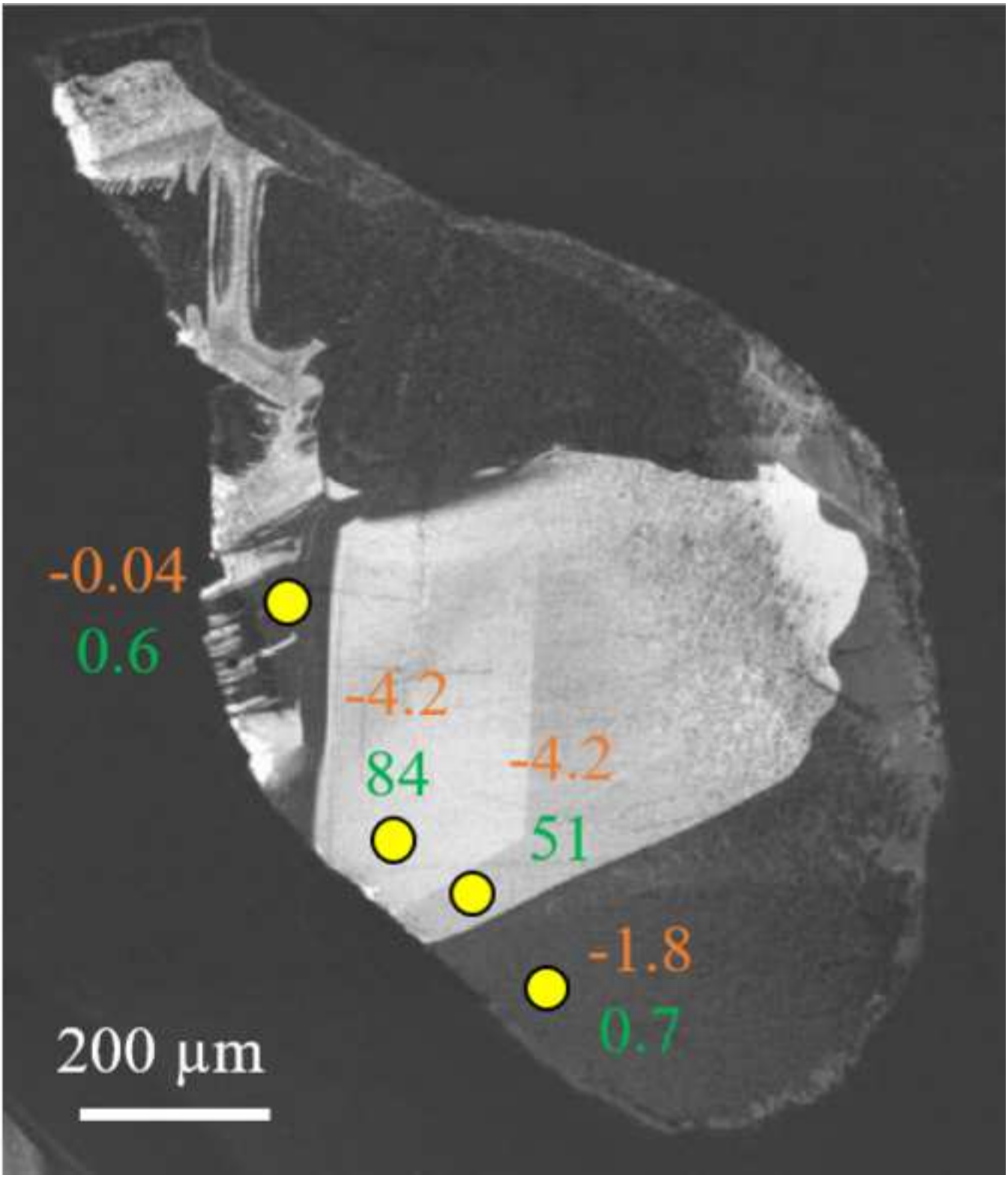

Figure 10

Click here to access/download;Figure;Figure 10.tif

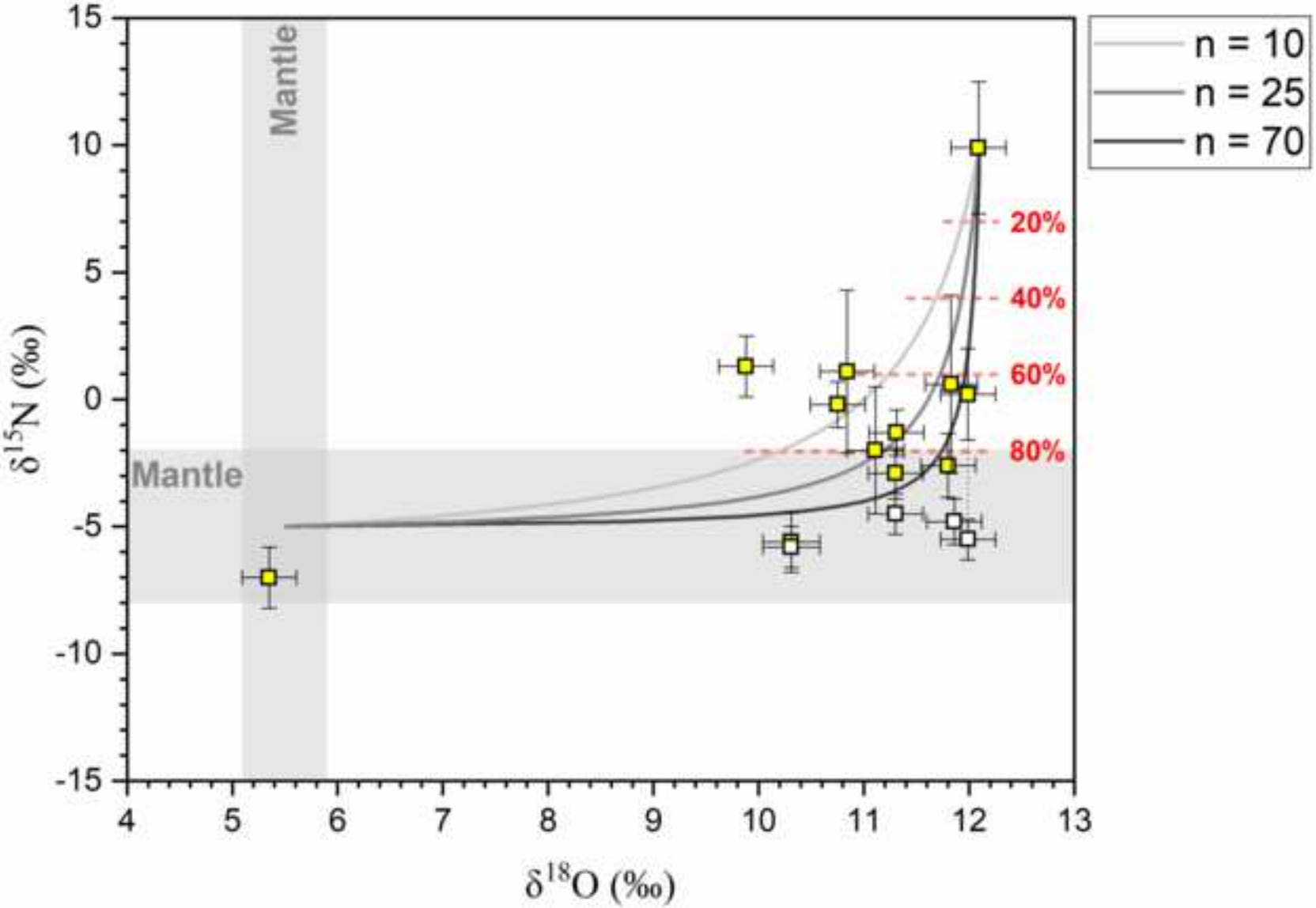

Fig. 1. Ti versus Na (apfu) for garnet inclusions in Koidu diamonds. Except for one garnet with a minor majorite component, garnets show a crude positive correlation (R^2 = 0.33) between Ti and Na.

Fig. 2. Al versus Ti (apfu) in garnet inclusions in Koidu diamonds, based on a formula unit containing twelve oxygen atoms. Al and Ti are strongly negatively correlated (R^2 = 0.81). The outlier with high Ti content is the mildly majoritic garnet.

Fig. 3. Covariation between Al+Cr and Si in garnets, based on a formula unit containing twelve oxygen atoms. Al+Cr decrease with increasing Si, indicating increasing pressure. Symbol colour represents the depths (km) corresponding to equilibration pressures reported in literature: triangles are data from high pressure experiments conducted by Akaogi and Akimoto (1979); squares are data from high pressure experiments conducted by Irifune et al. (1986) and Irifune (1987); circles are data compiled by Collerson et al. (2010) for garnet inclusions in diamonds worldwide. Black diamond symbols represent the chemical compositions of garnet inclusions in this study. The position of the dashed line, indicating a depth of 220 km (lithosphere-asthenosphere boundary of the West African Craton; Smit et al., 2016), is estimated from the garnet inclusions compiled by Collerson et al. (2010). Estimated pressures for garnet 140-2-1 is 7.8–8.2 GPa (Collerson et al., 2010; Beyer and Frost, 2017), corresponding to a depth between 250 and 260 km.

Fig. 4. REE concentrations in eclogitic garnets from Koidu diamonds normalized to CI-chondrite (McDonough and Sun, 1995). (a) Three garnet inclusions with discernible negative Eu anomalies. (b) Other garnet inclusions lacking obvious Eu anomalies. Garnets from diamond 138-7 (black) are different from other garnets in this study through their negative $MREE_N$-$HREE_N$ slopes with Lu_N < 10. Two garnets (black dashed lines) from diamond 138-7 have discernible positive Eu anomalies. Inset shows three garnets (138-3-1, 138-5-1 and 138-11-1) that follow a clear trend of decreasing Ca# with decreasing $\delta^{18}O$ values (see Fig. 7b).

Fig. 5. Distribution of $\delta^{18}O$ values in garnet inclusions from Koidu diamonds. The bin size for the histogram is 0.25 ‰. The region shaded in grey indicates the canonical $\delta^{18}O$ range of the mantle (+5.5 ± 0.4 ‰; Mattey et al., 1994). The $\delta^{18}O$ values of garnets in this study range from +5.4 to +12.1 ‰, with a mode of +11.8 ‰. Gabbroic garnet 138-7-3 has the lowest $\delta^{18}O$ value (+5.4 ‰), which falls within the mantle range.

Fig. 6. Oxygen isotope compositions ($\delta^{18}O$) of eclogitic garnet inclusions in diamonds from Koidu (this study), Damtshaa (Ickert et al., 2013), Argyle (Schulze et al., 2013), Finsch (Lowry et al., 1999), Siberian placer (Zedgenizov et al., 2016), Jericho (Smart et al., 2012) and the Guaniamo placer deposit ($\delta^{18}O$ values of multiple garnet inclusions in one single diamond; Schulze et al., 2004). The grey shaded region indicates the canonical $\delta^{18}O$ range of the mantle (+5.5 ± 0.4 ‰; Mattey et al., 1994).

Fig. 7. Covariations of oxygen isotope composition ($\delta^{18}O$) and molar Mg# (a), Ca# (b) and Cr# (c) in Koidu garnet inclusions (the gabbroic garnet is shown in blue, other garnets are shown in orange). Three garnets (138-3-1, 138-5-1 and 138-11-1; grey background) with clear correlations between $\delta^{18}O$ and major element compositions are shown with symbols following Fig. 4b. The region shaded in grey indicates the canonical $\delta^{18}O$ range of the mantle (+5.5 ± 0.4 ‰; Mattey et al., 1994). Garnets show a well-defined negative correlation (R^2 = 0.77) between Cr# and $\delta^{18}O$ values.

Fig. 8. Oxygen isotope composition ($\delta^{18}O$) of garnet inclusions and carbon isotope composition ($\delta^{13}C$) of their host diamonds in this study. Average $\delta^{18}O$ and $\delta^{13}C$ values of multiple analyzed spots of individual garnet grains and diamond fragments are shown. Four diamonds (138-5, 138-9, 143-2 and 146-2) have a core-rim structure and are linked by dashed tie-lines, with $\delta^{13}C$ values of the rims being indicated by white squares and core-zone values by yellow squares. Error bars reflect total uncertainties (95% confidence level) for the $\delta^{18}O$ and $\delta^{13}C$ values of each sample and for $\delta^{13}C$ are smaller than the symbol size. Also shown are $\delta^{13}C$ and $\delta^{18}O$ values of lithospheric (black)/sublithospheric (red) diamonds and their garnet inclusions from Argyle (Schulze et al., 2013), Damtshaa (Ickert et al., 2013), Siberian placers (Zedgenizov et al., 2016), Finsch (Lowry et al., 1999), Jagersfontein (Ickert et al., 2015) and Collier/Juina (Burnham et al., 2015).

Fig. 9. Cathodoluminescence image of diamond 140-2-1 showing inner and outer growth zones with distinct $\delta^{13}C$ values (orange; ‰) and nitrogen concentrations (green; at.ppm).

Fig. 10. Oxygen isotope composition ($\delta^{18}O$) of eclogitic garnet inclusions and nitrogen isotope composition ($\delta^{15}N$) of their host diamonds in this study. Average $\delta^{18}O$ and $\delta^{15}N$ values of multiple analyzed spots of individual garnet grains and diamond fragments are shown for each sample. Four diamonds (138-5, 138-9, 143-2 and 146-2) have a core-rim structure and are linked by dotted tie-lines, with the compositions of the rims indicated by white squares and core analyses by yellow squares. Error bars reflect total uncertainties (95% confidence level) for the $\delta^{18}O$ and $\delta^{15}N$ values of each sample. Solid lines indicate mixing arrays calculated using different $(O/N)_{AOC}/(O/N)_{mantle}$ ratios denoted by n: (light grey) n = 10; (dark grey) n = 25; and (black) n = 70. Red dashed lines indicate the percentages of nitrogen contributed by the mantle.